

Original Article

Bioactive components and the molecular mechanism of Shengxian Decoction against lung adenocarcinoma based on network pharmacology and molecular docking

Ruijiao Yuan¹, Kejuan Li¹, Qi Li¹, Chun Wang¹, Hong Zhang¹, Lihong Ge¹, Yifeng Ren³, Fengming You²

¹College of Life Science, Sichuan Normal University, Chengdu, Sichuan, China; ²Traditional Chinese Medicine (TCM) Regulating Metabolic Diseases Key Laboratory of Sichuan Province, Hospital of Chengdu University of Traditional Chinese Medicine, Chengdu, Sichuan, China; ³Hospital of Chengdu University of Traditional Chinese Medicine, Chengdu, Sichuan, China

Received August 16, 2023; Accepted November 22, 2023; Epub December 15, 2023; Published December 30, 2023

Abstract: Objective: The aim of this study was to identify the active components of Shengxian Decoction (SXT) and to elucidate the multi-component, multi-target, and multi-pathway regulatory mechanisms underlying the efficacy of SXT in treating lung adenocarcinoma (LUAD). Methods: The effects of SXT extract on proliferation, migration, and invasion capabilities of human LUAD cells were determined through 3-(4,5-dimethylthiazol-2-yl)-2,5-diphenyltetrazolium bromide (MTT), wound healing, and Transwell assays. High-Performance Liquid Chromatography (HPLC) was employed to pinpoint the primary active constituents of SXT. The SXT-active component-target-pathway network and protein-protein interaction (PPI) network were constructed based on network pharmacology. Gene Ontology (GO) and Kyoto Encyclopedia of Genes and Genomes (KEGG) pathway analyses were performed using DAVID. The clinical significance of key targets was assessed using several external databases, and molecular docking confirmed the binding affinities between key targets and SXT active components. Results: SXT significantly inhibited the proliferation, migration and invasion of human LUAD cells. HPLC identified and quantified seven active SXT components. Network pharmacology yielded 197 targets, 128 signaling pathways, and 448 GO terms. The PPI network and external validation underscored 13 key targets significantly associated with the influence of SXT on LUAD progression. Molecular docking demonstrated strong interactions between SXT active components and key targets. Conclusion: SXT treats LUAD through a multifaceted approach involving various components, targets, and pathways. This research offers novel insights into the constituents and molecular mechanisms of SXT in LUAD therapy.

Keywords: Shengxian Decoction (SXT), lung adenocarcinoma (LUAD), active components, network pharmacology, molecular docking

Introduction

Epidemiological data indicate that lung cancer is the leading cause of cancer-related mortality globally, with five-year survival rates ranging from 4% to 17% [1, 2]. According to China's 2021 statistics, lung cancer was the most prevalent and lethal cancer in 2015, with non-small cell lung cancer (NSCLC) accounting for nearly 85% of cases [1, 3]. Among NSCLC histological subtypes, lung adenocarcinoma (LUAD) is the most common.

Currently, LUAD patients may undergo surgical resection, thoracic radiotherapy, cytotoxic chemotherapy, immunotherapy, targeted therapy,

or combinations thereof. However, these treatments can have adverse effects that restrict their application [4]. Traditional Chinese Medicine (TCM) has emerged as a viable alternative for LUAD treatment due to its efficacy and lower side effects [5]. Nevertheless, the complexity of TCM, involving multiple components and targets, poses challenges in elucidating its mechanisms of action. Advances in computational technology have facilitated network pharmacology and molecular docking to predict active components, key targets, and mechanisms of TCM action, significantly reducing drug development costs and offering new insights into the material basis and mechanisms of TCM [6-8].

Potential mechanism of Shengxian Decoction against lung adenocarcinoma

Shengxian Decoction (SXT), a classic TCM formula commonly used for the syndrome of pectoral Qi sinking, is comprised of five herbs including Astragali Radix (A. radix), Anemarrhenae Rhizoma (A. rhizoma), Bupleuri Radix (B. radix), Platycodonis Radix (P. radix) and Cimicifugae Rhizoma (C. rhizoma) [9]. The constituent herbs, and phytochemicals they contain, have also been reported to be effective in cancer prevention and treatment, including LUAD. A. radix and B. radix, for example, have been used alongside radiotherapy to improve survival rates and lessen chemotherapy toxicity in lung cancer [10, 11]. A. rhizoma and C. rhizoma extracts are rich in various active compounds with antitumor activity against the LUAD cell line A549 [12, 13], and P. radix is a component of various TCM formulas for lung tumor treatment [14]. Furthermore, our earlier findings revealed that SXT serum inhibit A549 cell proliferation in vitro and that SXT administration significantly reduced tumor growth in A549 xenografts in nude mice [15]. However, the chemical composition of SXT and the possible mechanisms associated with its effect remain unclear.

This study first assessed the inhibitory effects of SXT extract on human LUAD cells through in vitro assays. Subsequently, the primary active components of SXT were identified using High-Performance Liquid Chromatography (HPLC). The key targets of SXT active components for LUAD treatment were predicted using network pharmacology and validated with external databases. Lastly, the interactions between the active components of SXT and key targets in LUAD were determined through molecular docking. The methodologies employed in this study are depicted in **Figure 1**.

Materials and methods

Preparation of SXT extract

The botanical drug mixture of A. radix, A. rhizoma, B. radix, P. radix and C. rhizoma (12:6:3:3:2) was soaked in distilled water (v:v = 1:12) for 2 h and then boiled for 30 min. The decoction was filtrated and the resulting residues were subsequently collected for two additional decoctions, each with 8 volumes of distilled water and boiled for 30 min. The sum of the decoctions was condensed using reduced pressure (-0.07~-0.08 MPa) at 70°C. The resul-

tant concentrate was freeze-dried and labeled as SXT extract (extraction rate: 38.95%). The obtained SXT extract was stored at -20°C before chemical and pharmacological studies.

Cell line and culture

Human LUAD cell lines (A549 and NCI-H1299) and human embryonic lung fibroblasts WI-38 were obtained from the American Type Culture Collection (ATCC). The cells were cultured in Ham's F-12K medium (A549 cells), RPMI-1640 medium (NCI-H1299 cells), and MEM medium (WI-38 cells), respectively. The aforementioned medium items were acquired from the vendor Procell, and all of the mediums were supplemented with 10% fetal bovine serum (Biosharp, China) and 1% penicillin-streptomycin solution (Procell, China). The cells were subjected to incubation in a controlled environment consisting of 5% CO₂/95% air at 37°C within a humidified incubator.

Cell viability assay and morphology observations

The 3-(4,5-dimethylthiazol-2-yl)-2,5-diphenyltetrazolium bromide (MTT) assay was used to assess the cell viability. The cells in logarithmic growth phase were inoculated in 96-well plates at a density of 2×10^3 cells well⁻¹ and allowed to adhere overnight. Cells were then treated with culture medium containing 0, 2, 4, 6, 8, and 10 mg/mL SXT extract. After 24 h or 48 h of treatment, cells were treated with 5 mg/mL MTT solution, incubated at 37°C for 4 h, and then the MTT solution was replaced with 150 μ L of DMSO for complete dissolution of formazan crystals. The absorbance (OD) at 490 nm was measured by SpectraMax 190 absorbance plate reader (Molecular Devices, USA).

For morphological observation, cells (1×10^5 cells well⁻¹) were seeded in 6-well plates and allowed to adhere overnight. The cells were subsequently treated with fresh medium containing 0, 2, 4, 6, 8, and 10 mg/mL SXT for 48 h. Cell morphology was recorded under a $\times 100$ microscope using DM IL LED inverted laboratory microscope (Leica Microsystems, Germany).

Wound healing assay

A wound healing assay was performed to evaluate the effect of SXT extract on A549

Potential mechanism of Shengxian Decoction against lung adenocarcinoma

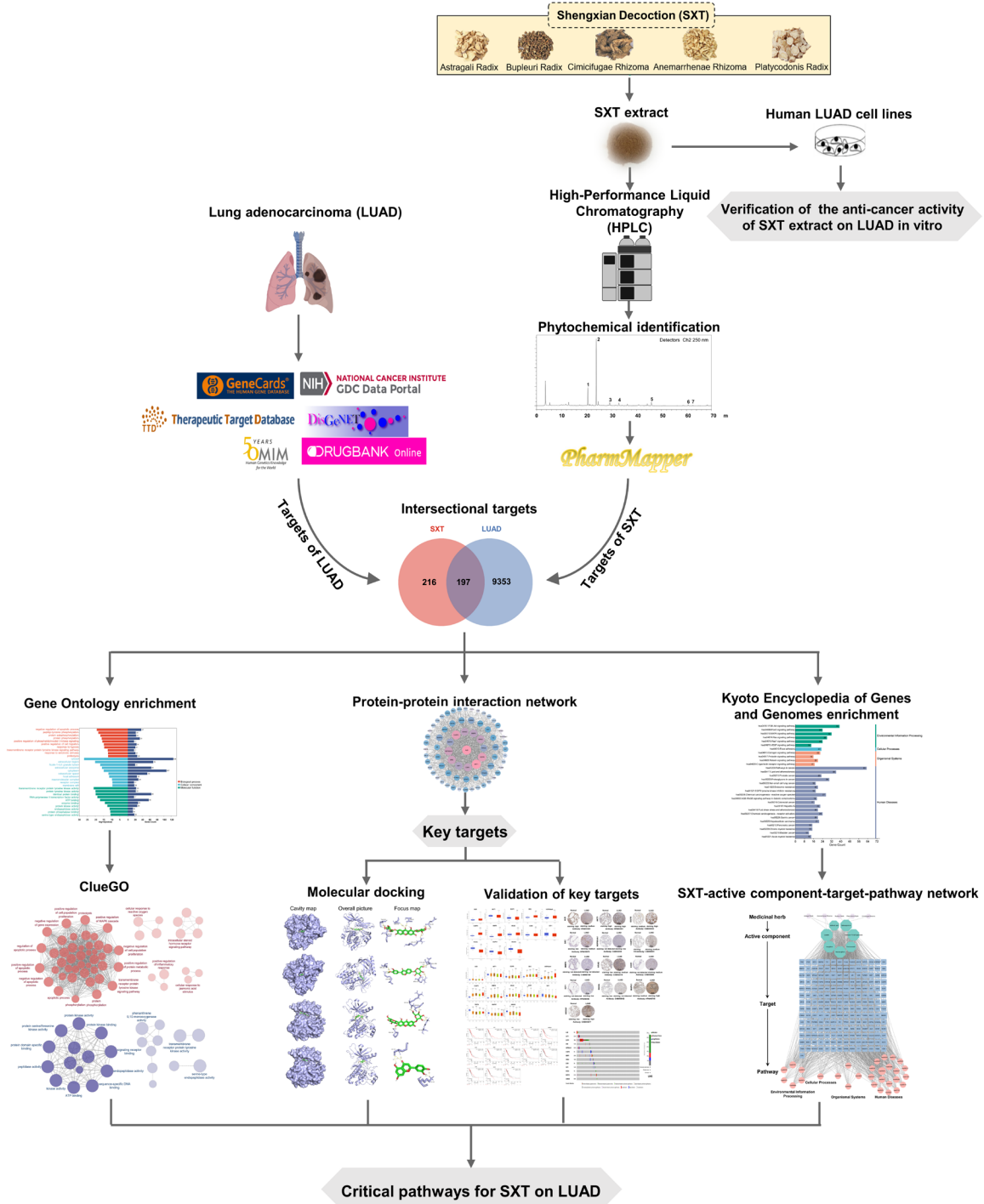


Figure 1. The schematic diagram of the network pharmacology of Shengxian Decoction (SXT) for lung adenocarcinoma (LUAD).

and NCI-H1299 cell motility. Cells were seeded in 6-well plates at a density of 1×10^5 cells well⁻¹ and cultured overnight. The cell monolayer was scraped with 200 μ L pipette tips at

90% confluency, and cell debris was removed by washing with PBS twice. Cells were then cultured in serum-reduced media (2% FBS) with 5 mg/mL SXT extract. Cell migration into the

Potential mechanism of Shengxian Decoction against lung adenocarcinoma

Table 1. Quantitative analysis of SXT extract by HPLC

Active component	Content (mg/g)	Regression equation	Correlation coefficient (R ²)	Linear range (µg/mL)
Neomangiferin	1.0270 ± 0.0222	Y = 35038X-916.22	1	0.3125-40
Mangiferin	3.5320 ± 0.0775	Y = 73591X+58.217	0.9999	0.3125-40
Calycosin 7-O-Glucoside	0.4264 ± 0.0143	Y = 42342X+3521.4	1	0.3125-40
Isoferulic acid	0.2700 ± 0.0180	Y = 59103X-2313.6	1	0.3125-40
Luteolin	0.2958 ± 0.0188	Y = 66345X-5221.5	1	0.3125-40
Formononetin	0.0454 ± 0.0012	Y = 112880X+2208.6	1	0.1-40
Saikosaponin A	6.4690 ± 0.1189	Y = 585.38X+265.33	0.9997	2.5-320

Note: mean ± SD; n = 6; SXT, Shengxian Decoction; HPLC, High-Performance Liquid Chromatography.

scratched region was examined and recorded at 0, 24, and 48 h and wound closure speed was assessed using ImageJ software.

Cell invasion assay

The Transwell invasion assay was used to assess the effect of SXT extract on the invasiveness of A549 and NCI-H1299 cells. A Transwell chamber insert (BD Corporation, Franklin Lakes, NJ, United States) with 300 µg/mL Matrigel was used in this study. 2×10^4 cells suspended in 100 µL of serum-free culture medium containing 5 mg/mL SXT extract were added into the top invasion insert, while 600 µL of culture medium with 10% FBS was loaded into the well below. After 24 h of incubation, invasive cells that passed through the filter were fixed with methanol and stained with 1% crystal violet. The inserts were rinsed, air-dried, viewed, and photographed. Invasion activity was assessed by counting at least five random fields in each chamber at $\times 200$ magnification.

Preparation of SXT extract sample and mixed-standard solutions

SXT extract (6 mg/mL) and the stock solutions of seven standard substances (neomangiferin, mangiferin, calycosin 7-O-glucoside, isoferulic acid, luteolin, formononetin and saikosaponin A) were carefully prepared in specific concentrations with methanol. Mixed-standard solutions were prepared by mixing the individual reference stock solutions and the concentrations for each standard substance are shown in **Table 1**. All samples were filtered through 0.22 µm microporous membrane prior to HPLC injection.

Quantification of main active components in SXT by HPLC

The chromatographic study of SXT extract was performed using an LC-2030C HPLC (Shimadzu, Japan). Separation was accomplished by using an Agilent ZORBAX SB-C18 (4.6 × 250 mm, 5 µm) column (Agilent Technologies, USA). The mobile phase was composed of acetonitrile (solvent A) and 0.2% formic acid aqueous solution (solvent B) with gradient elution: 0~5 min, 99% B; 5~20 min, 99%~83% B; 20~25 min, 83%~80% B; 25~33 min, 80%~77% B; 33~40 min, 77%~70% B; 40~50 min, 70%~67% B; 50~65 min, 67%~50% B; 65~70 min, 50%~30% B. The flow rate was maintained at 0.8 mL/min, while the column temperature was set to 30°C and the injection volume was 10 µL. The discovery of the peak occurred at a wavelength of 250 nm.

The experiment involved generating a standard curve using a concentration gradient. This was done to evaluate the linear correlation between the concentration of the analyte (X) and the corresponding peak areas obtained (Y). An external standard method was used to determine the amount of each detected compound. The results were expressed as mg/g dry weight.

Statistical analysis

In the quantitative identification of SXT extract by HPLC, six replicate determinations of SXT extract were performed, and the other experiments were performed in triplicates. All of the results were presented as the mean ± standard deviation (SD). One-way ANOVA was used for multiple comparisons, and the Tukey method was used to compare any two groups of data. Significant differences were determined at $*P \leq$

Potential mechanism of Shengxian Decoction against lung adenocarcinoma

0.05, $**P \leq 0.01$, and $***P \leq 0.001$. All data were analyzed using GraphPad Prism 9 (San Diego, CA, United States).

Target prediction of SXT active components

PharmMapper [16-18] (<http://lilab-ecust.cn/pharmmapper/index.html>) matches active component with the internal pharmacophores model database for reverse pharmacophores to identify potential drug targets to obtain the corresponding targets of the active components. The Structure-Data File of SXT active components were searched in the PubChem database (<https://pubchem.ncbi.nlm.nih.gov/>) then entered the PharmMapper to obtain the predicted genes for SXT active components. The gene symbol names were converted by UniProt (<https://www.uniprot.org/>) database, and duplicates were removed.

LUAD-related targets prediction

From the transcriptome expression profiles of LUAD retrieved from The Cancer Genome Atlas Program (TCGA) database (<http://cancergenome.nih.gov/>), samples of RNA expression data were extracted, which included 59 normal samples and 539 LUAD tumor samples. Later, the data were processed using the edge R package, and $**P \leq 0.01$ and $|\log_2 FC| > 2$ were used as screening criteria to analyze the above differentially expressed genes. To improve the comprehensiveness and reliability of data collection on targets relevant to this disease, genes data from five online platforms were supplemented. LUAD-related targets were retrieved from GeneCards (<https://www.genecards.org/>), DisGeNET (<https://www.disgenet.org/>), Online Mendelian Inheritance in Man (OMIM, <https://omim.org/>), Therapeutic Target Database (TTD, <http://db.idrblab.net/ttd/>) and DrugBank (<https://www.drugbank.ca/>) with “LUAD” and “lung cancer” as the keyword for searching. These disease genes were then compared with LUAD differentially expressed genes obtained through the TCGA database so that all genes obtained were associated with LUAD progression. All the genes in each database were combined together and then duplicates were removed. SXT active component targets and LUAD targets were inputted to draw Venn diagram, and the common targets were collected.

Gene Ontology (GO) and Kyoto Encyclopedia of Genes and Genomes (KEGG) pathway enrichment analysis

GO and KEGG enrichment analysis of common targets of SXT active components for LUAD was performed using the DAVID (<https://david.ncifcrf.gov/>) database. The top 30 terms were plotted at Bioinformatics online tools (<https://www.bioinformatics.com.cn>). ClueGO is used as a Cytoscape plug-in to analyze the interrelationship of terms and functional groups in biological networks and to present them as a network diagram. The GO enrichment results obtained from the DAVID database were imported into ClueGO for classification and grouping by function, where Biological Processes (BPs) and Molecular Functions (MFs) of GO analysis were highlighted.

Constructed SXT-active component-target-pathway network

SXT-active component-target-pathway network was built with Cytoscape 3.9.0.

Construction of network

A protein-protein interaction (PPI) network was constructed by importing the common targets to the STRING database (<https://www.string-db.org/>) with a confidence score set to 0.4, the species restricted to “Homo sapiens”, and concealing free points. Cytoscape 3.9.0 was used to visualize the PPI network and topological analysis was performed by Cytoscape-CytoNCA [19]. Degree centrality (DC), Closeness centrality (CC), and Betweenness centrality (BC) are used to measure the importance of the protein in the PPI network. The top 13 targets with the largest DC value were recognized as key targets for SXT active components in the treatment of LUAD.

External validation of key targets

In this study, we use UALCAN (<http://ualcan.path.uab.edu>) [20, 21] to explore the association of the key target mRNA expression in sample type and cancer stage. Significant difference was considered at $*P \leq 0.05$; $**P \leq 0.01$; $***P \leq 0.001$. To investigate the expression of key targets in LUAD tissues, we analyzed the key targets in the Human Protein Atlas database (HPA, <https://www.proteinatlas.org/>)

Potential mechanism of Shengxian Decoction against lung adenocarcinoma

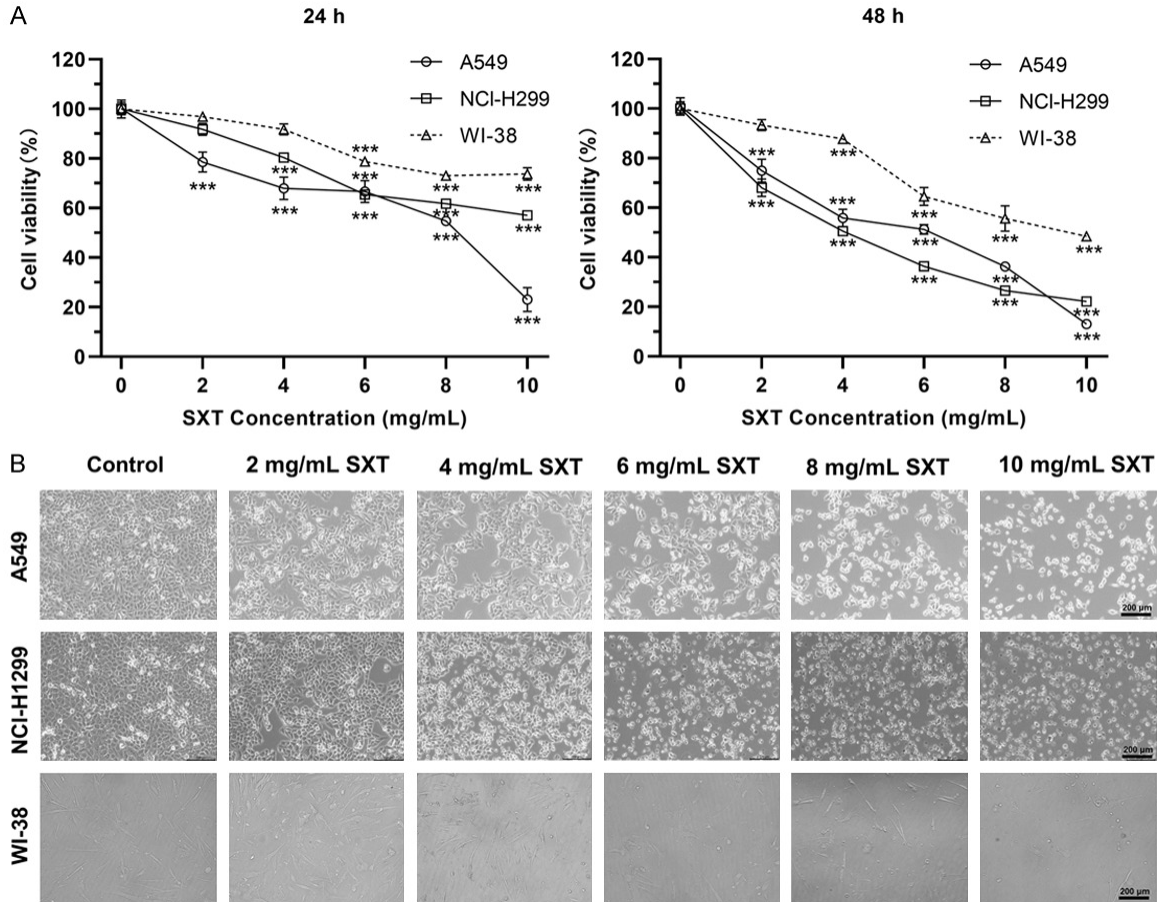


Figure 2. Cytotoxicity effects of Shengxian Decoction (SXT) extract on human lung adenocarcinoma cells and non-carcinoma cells. A. Cell viability assays of control and 24 h/48 h SXT extract-treated cells showing a dose-dependent cytotoxicity in A549 and NCI-H1299, while the killing effect on WI-38 cells was relatively light (mean \pm SD; $n = 3$). $***P \leq 0.001$; B. Morphological changes in each group of cells after 48 h SXT extract treatment was observed under $\times 100$ microscope (scale bar, 200 μm).

[22]. Overall survival (OS) analysis was carried out on the Kaplan-Meier mapper database (<http://kmplot.com/analysis/>) [23]. The hazard ratio (HR) and log rank P value were calculated and displayed in the graph, and a log rank $*P \leq 0.05$ and $**P \leq 0.01$ were set as a significant difference. The LUAD (TCGA, PanCancer Atlas) dataset containing 566 samples was selected for analysis in cBioPortal (<https://www.cbioportal.org/>). Information on the genetic alterations of the key targets was obtained.

Molecular docking validation of SXT active components with key targets

The Structure-Data Files of SXT active components were converted to the mol2 format using Chem3D software. The crystal structures of key targets were obtained from the RCSB protein

database (PDB, <http://www.rcsb.org/>). Water molecules, ligands and other hetero atoms were removed using PyMOL. AutoDock Vina was used to dock SXT active components on LUAD molecules to explore the binding pose and interactions between the drug and the target protein.

Results

Anti-proliferative effect of SXT extract on LUAD cells (A549 and NCI-H1299) and human embryonic lung fibroblasts (WI-38)

MTT assays were performed to investigate the anti-cancer potential of SXT extract against human LUAD cells (A549 and NCI-H1299) and human embryonic lung fibroblasts WI-38. As shown in **Figure 2A**, compared to control, SXT

Potential mechanism of Shengxian Decoction against lung adenocarcinoma

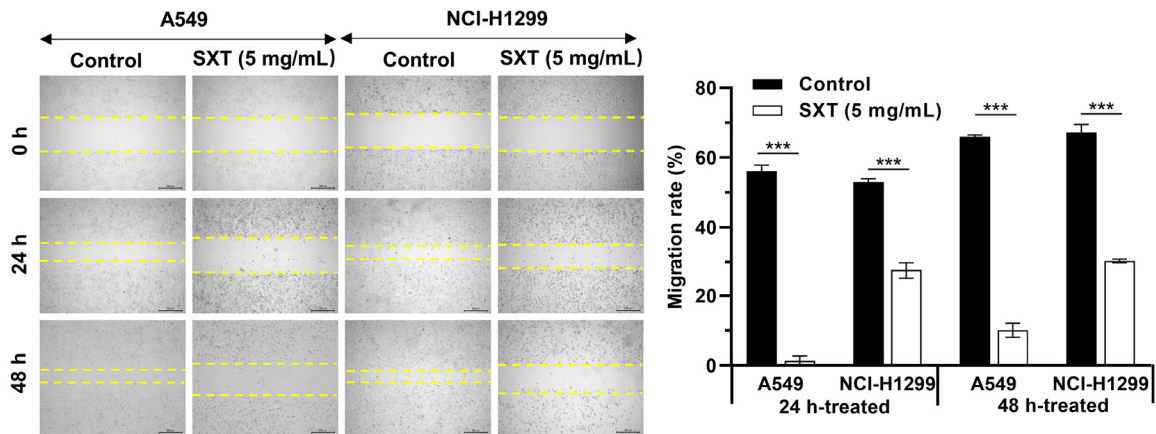


Figure 3. Effect of SXT extract on the migration capacity of A549 and NCI-H1299 cells. Wound healing assay and its quantitation showing strong inhibition with 5 mg/mL of SXT extract treatment (magnification, $\times 40$; scale bar, 200 μm). Quantitative data are represented as mean \pm SD ($n = 3$). $***P \leq 0.001$. SXT, Shengxian Decoction.

extract exhibited significant cytotoxic effects on both LUAD cell lines in a dose- and time-dependent manner, while the killing effect on WI-38 cells was relatively light. The IC_{50} values of SXT extract against A549/NCI-H1299/WI-38 cells were determined to be 7.19/11.76/19.27 mg/mL and 4.33/3.81/9.22 mg/mL after 24 h and 48 h of treatment, respectively. Microscopic examination of cell morphology (**Figure 2B**) highlighted the selective cytotoxic activity of SXT extract on LUAD cells juxtaposed with normal, non-cancerous cells within a concentration of 6 mg/mL over 24 h of treatment.

SXT extract inhibits migration and invasion of LUAD cells

We next examined the effect of SXT extract on LUAD cell migration and invasion as these cells are known for their high metastatic potential. **Figure 3** illustrates that 48 h of SXT extract (5 mg/mL) treatment significantly reduced A549 and NCI-H1299 cell migration by 55.87% and 36.77%, respectively. The effect was evident that SXT extract significantly ($***P \leq 0.001$) inhibited the motility of A549 and NCI-H1299 cells migrating into the wound area compared to control cells. **Figure 4** demonstrates that following 24 h of SXT extract (5 mg/mL) treatment, A549 and NCI-H1299 invasiveness significantly ($***P \leq 0.001$) reduced by more than 90%. These findings indicate the potential for SXT extract to inhibit LAUD metastasis in vitro.

Identification of active components in SXT extract

The chemical fingerprint of the SXT extract was established using HPLC. Seven chemicals were used as standard samples for comparison with the SXT extract (**Figure 5A**). Analysis revealed several peaks (**Figure 5B**), indicating the presence of multiple substances. The active components of SXT were identified by comparing the retention times of major peaks with those of the standards. Peaks 1-7 in the SXT extract corresponded to neomangiferin, mangiferin, calycosin 7-O-glucoside, isoferulic acid, luteolin, formononetin, and saikosaponin A, respectively (**Figure 5C**). **Table 1** lists the concentrations of these compounds in the SXT extract, with saikosaponin A (6.47 mg/g) and mangiferin (3.53 mg/g) being the most abundant. These results suggest that the prepared SXT extract contains various active components, whose mechanism of action in LUAD treatment will be further explored using a network pharmacology approach.

Common targets of SXT active components and LUAD

The PharmMapper database provided 289 targets for neomangiferin, 288 for mangiferin, 286 for calycosin 7-O-glucoside, 260 for isoferulic acid, 288 for luteolin, 242 for formononetin, and 285 for saikosaponin A. After removing duplicates, 413 targets related to SXT active components were identified.

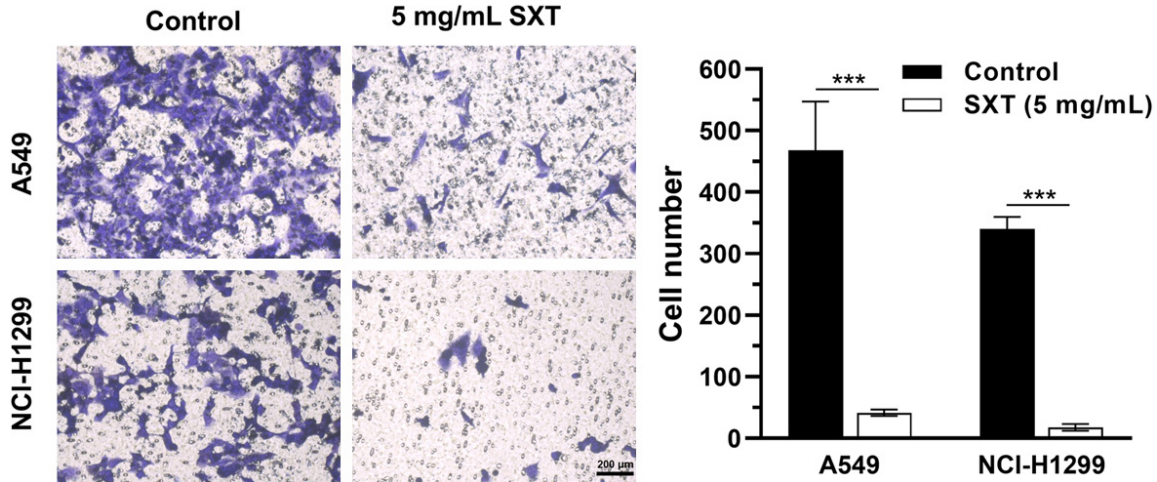


Figure 4. Effect of SXT extract on the invasion capacity of A549 and H1299 cells. Invasion assays and its quantitation showing strong inhibition with 24 h treatment of SXT extract (5 mg/mL) (magnification, $\times 200$; scale bar, 200 μm). Quantitative data are represented as mean \pm SD ($n = 3$). $***P \leq 0.001$. SXT, Shengxian Decoction.

The TCGA database yielded 598 samples, comprising 539 tumor and 59 normal samples. Analysis revealed 7365 differentially expressed genes, visualized in volcano plots with genes of increased expression in red and decreased expression in blue in LUAD tumor samples (**Figure 6A**). From the GeneCards, DisGeNET, OMIM, TTD, and DrugBank databases, 2007, 58, 1060, 227, and 82 LUAD-related targets were identified, respectively. After eliminating duplicates, 9550 targets related to LUAD were compiled. Ultimately, 197 common targets were derived from the intersection of drug- and disease-related targets (**Figure 6B**), suggesting that SXT active components modulates LUAD progression through these targets.

Biological process and pathway enrichment analysis

GO enrichment analysis of 197 common targets were assessed by DAVID to explore the dynamic activity of SXT active components in LUAD using a filtering threshold of $**P \leq 0.01$ (**Supplementary Table 1**). Analysis revealed 320 BPs including negative regulation of the apoptotic process and positive regulation of phosphoinositide 3-kinase (PI3K) signaling, 39 Cellular Components (CCs) involving the cytosol and extracellular region, and 89 MFs including transmembrane receptor protein tyrosine kinase activity. The top 10 related entries for BPs, MFs, and CCs are shown in a category

summary chart (**Figure 7A**). To further analyze the interrelationship of terms and functional groups in biological networks, 320 BPs and 89 MFs were analyzed separately using ClueGO to enrich for entries with similar groups, displayed as a network graph. As illustrated in **Figure 8**, the analysis of the most populated group in the functional enrichment network map of MFs highlighted the inclusion of kinase-related molecular functions, such as protein kinase binding and protein serine/threonine kinase activity. Additionally, apoptosis-related biological processes constituted a significant portion of the enrichment network graph, including the regulation of apoptotic processes. This suggests that the SXT active components might regulate cellular behavior, especially apoptosis, by regulating protein kinases.

Significantly relevant signaling pathways of 197 common targets were explored with KEGG enrichment analyses using DAVID. This analysis identified 128 pathways showing significant differences ($**P \leq 0.01$, **Supplementary Table 2**). The top 30 pathways with the highest $-\log_{10}$ (P value) were selected for visual analysis bioinformatics platform (**Figure 7B**). The results of the KEGG enrichment analysis included: 1) environmental information processing pathways such as the PI3K-protein kinase (Akt) signaling pathway, forkhead box protein O (FoxO) signaling pathway, and mitogen-activated protein kinase (MAPK) signaling pathway; 2) cellu-

Potential mechanism of Shengxian Decoction against lung adenocarcinoma

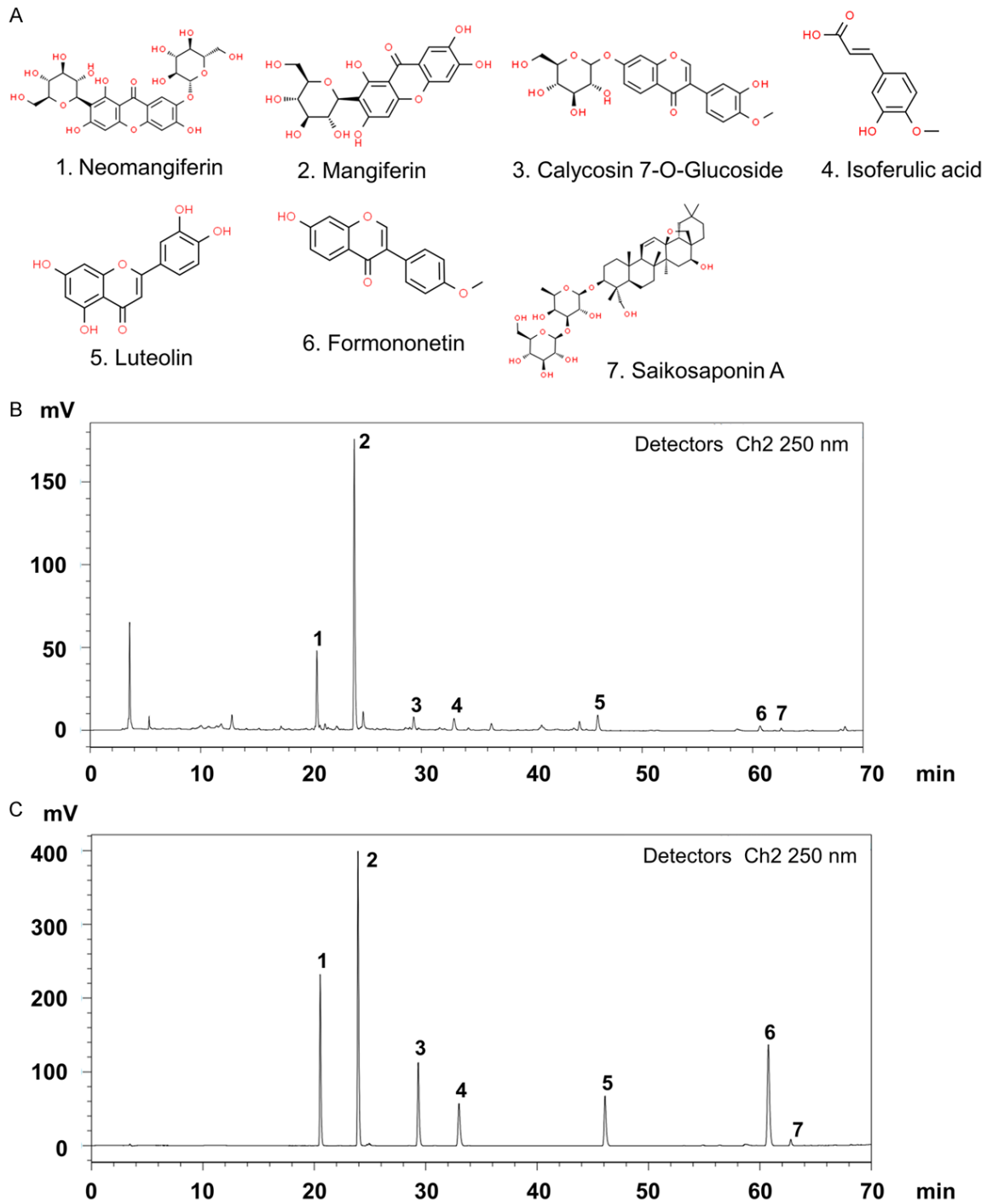


Figure 5. Identification of anti-cancer phytochemicals in SXT extract by HPLC analysis. A. Potential chemical compounds in SXT extract responsible for anti-cancer effect; B. HPLC chromatogram of SXT extract; C. HPLC chromatogram of mixed-standard substance; Peak assignment as follows: 1. Neomangiferin, 2. Mangiferin, 3. Calycosin 7-O-glucoside, 4. Isoferulic acid, 5. Luteolin, 6. Formononetin, 7. Saikosaponin A. SXT, Shengxian Decoction; HPLC, High-Performance Liquid Chromatography.

lar processes involving focal adhesion; 3) organismal systems involving the estrogen signaling pathway; and 4) human diseases path-

ways including those in cancer, NSCLC, and epidermal growth factor receptor (EGFR) tyrosine kinase inhibitor resistance. These findings

Potential mechanism of Shengxian Decoction against lung adenocarcinoma

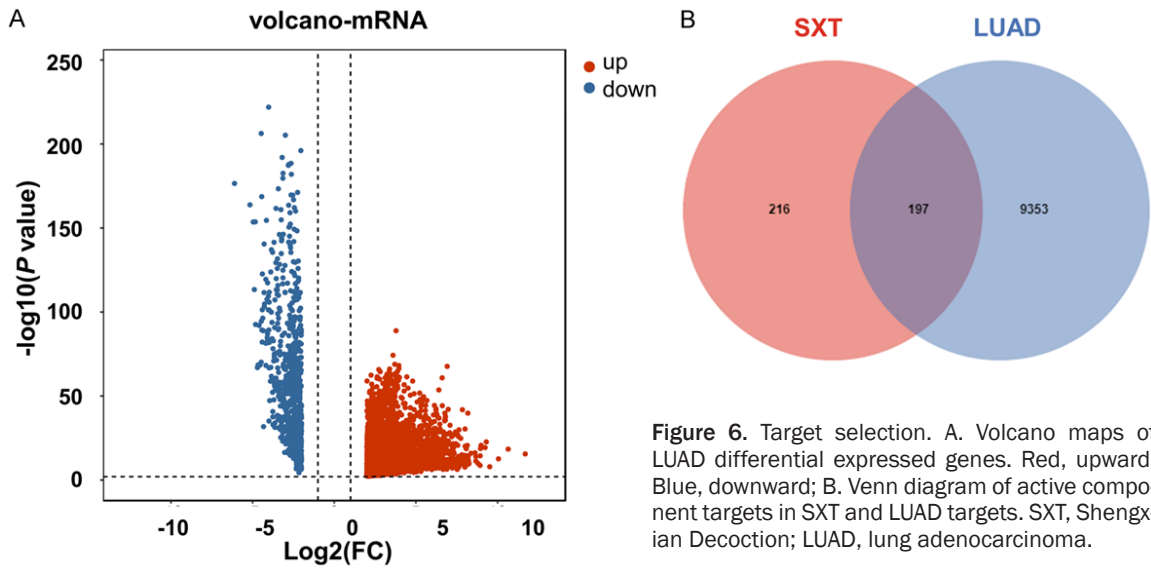
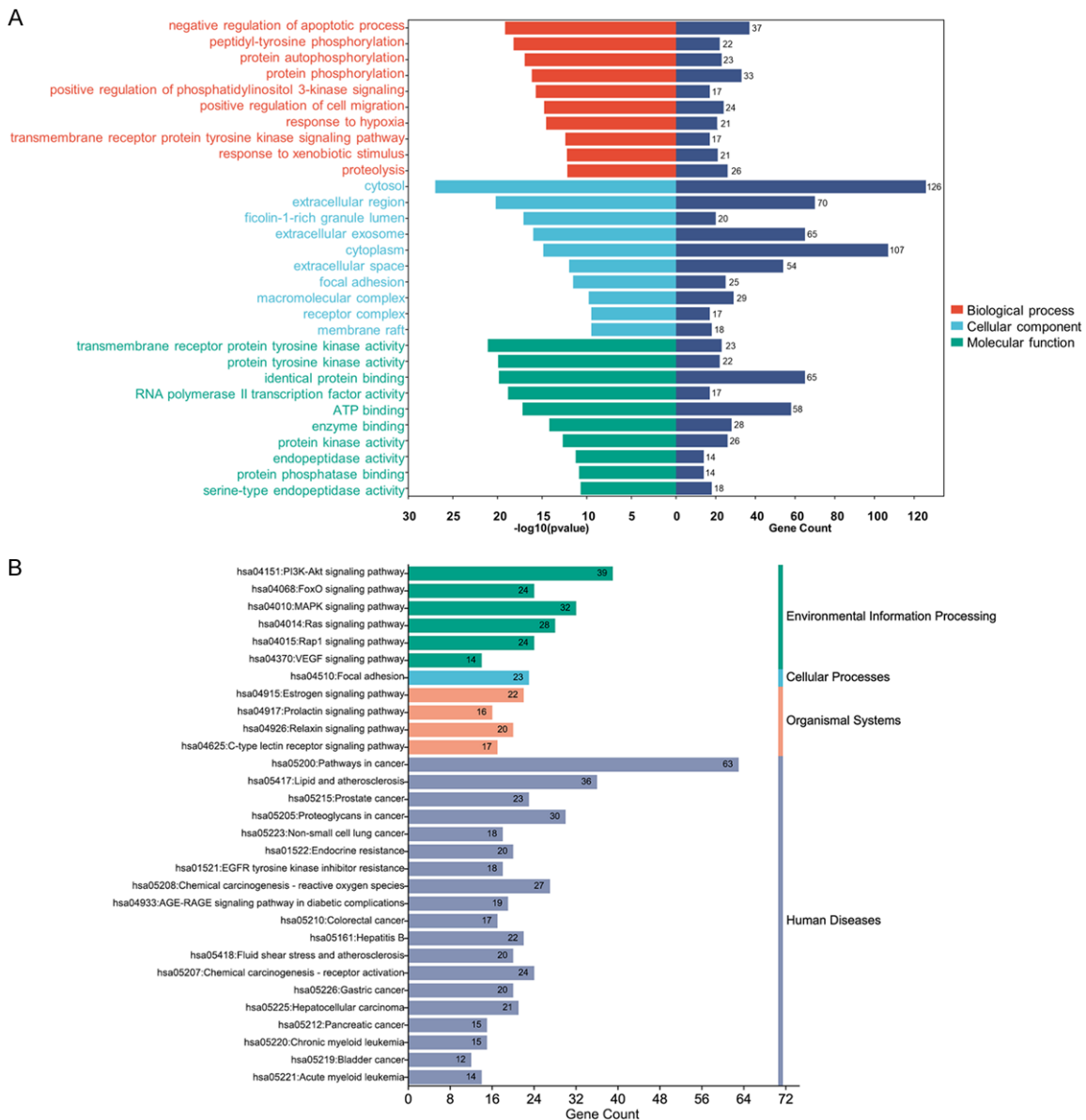


Figure 6. Target selection. A. Volcano maps of LUAD differential expressed genes. Red, upward; Blue, downward; B. Venn diagram of active component targets in SXT and LUAD targets. SXT, Shengxian Decoction; LUAD, lung adenocarcinoma.



Potential mechanism of Shengxian Decoction against lung adenocarcinoma

Figure 7. GO functional enrichment analysis and KEGG analysis of 197 common targets. A. The Bar chart of the top 10 terms of biological processes, cellular components and molecular functions extracted according to the *P* value based on GO enrichment analysis. In order to be able to show it in the figure, RNA polymerase II transcription factor activity and ligand-activated sequence-specific DNA binding to RNA polymerase II transcription factor activity were deleted in the GO analysis; B. The Bar chart of the top 30 terms extracted according to the *P* value based on KEGG enrichment analysis. GO, Gene Ontology; KEGG, Kyoto Encyclopedia of Genes and Genomes.

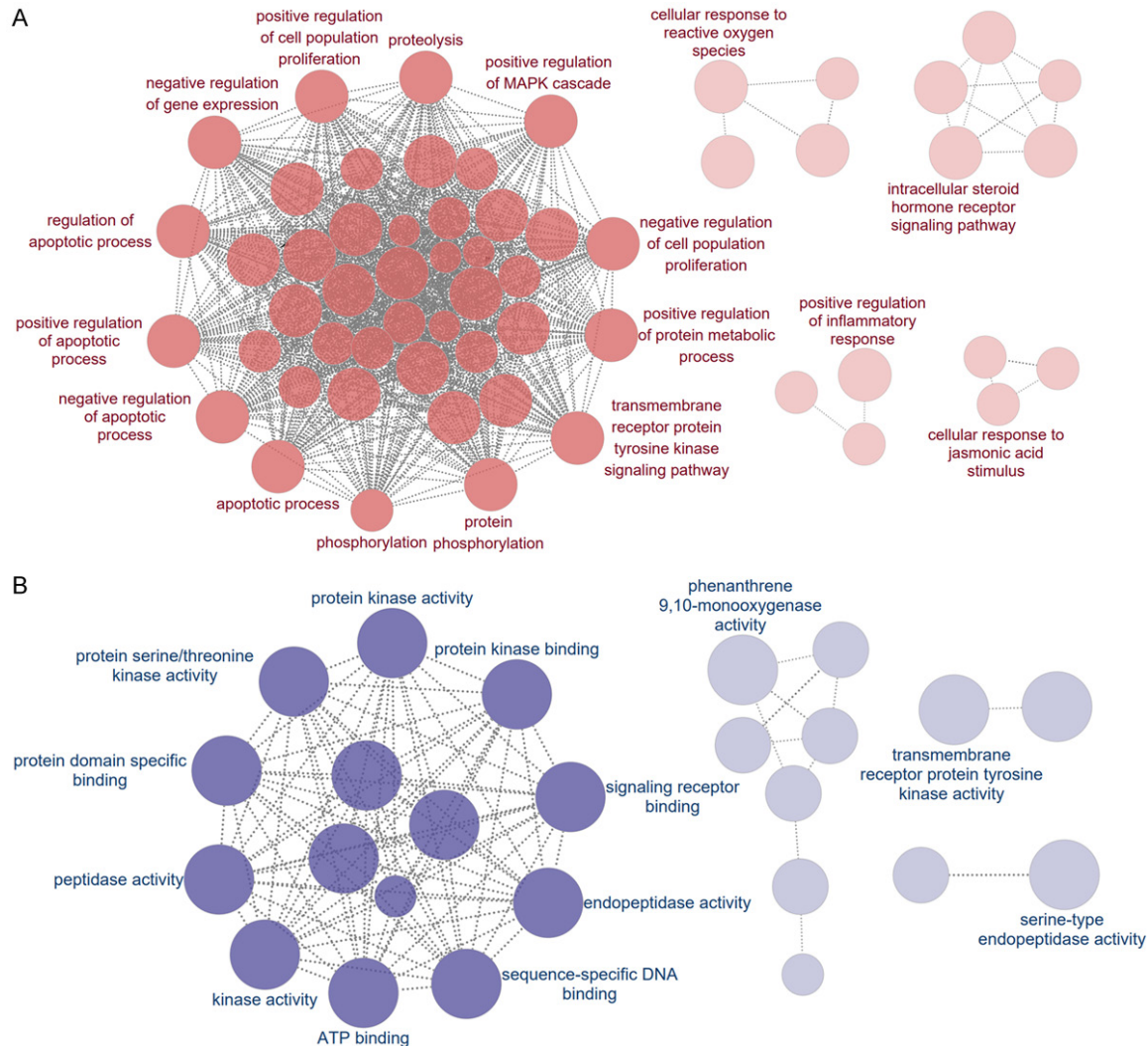


Figure 8. The interaction network of GO terms generated by the Cytoscape plug-in ClueGO. A. The functional networks with the most terms enriched by biological processes are shown; B. The functional networks with the most terms enriched by molecular functions are shown. The GO terms are rendered as nodes, with the size of the node representing importance. GO, Gene Ontology.

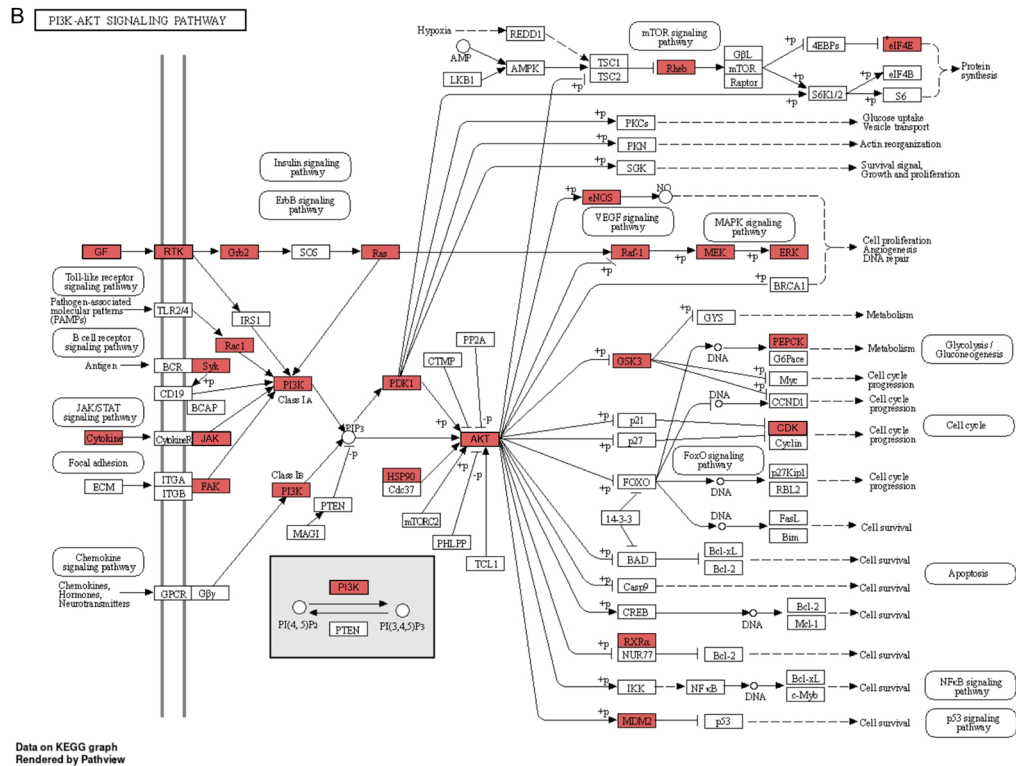
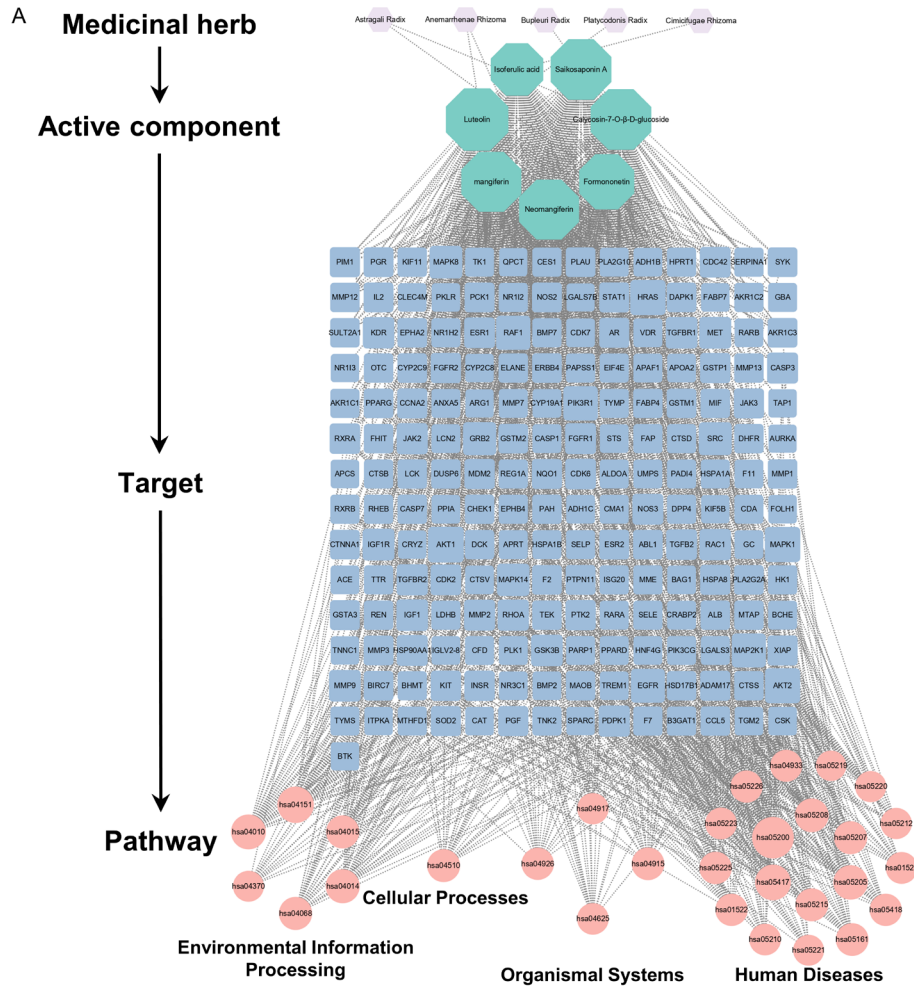
suggest that SXT active components may play a significant role in intervening these pathways in LUAD.

SXT-active component-target-pathway network

The SXT-active component-target-pathway network, depicted in **Figure 9A**, comprised 239

nodes, including 5 herbs, 7 active components, 197 common targets, and 30 KEGG enrichment pathway. Analysis of this network suggested that the therapeutic effect of SXT on LUAD is mediated through a complex interplay of multiple components, targets, and pathways. Notably, the PI3K-Akt signaling pathway emerged as the second most significantly

Potential mechanism of Shengxian Decoction against lung adenocarcinoma



Potential mechanism of Shengxian Decoction against lung adenocarcinoma

Figure 9. Construction and pathway analysis of the SXT-active component-target-pathway. A. SXT-active component-target-pathway. The nodes with different colors and shapes represent the herbs, components, targets, and pathways, and an edge is an association between the nodes; B. PI3K-Akt signaling pathway. The red nodes represent potential targets of SXT active component for the treatment of LUAD, arrows represent the activation effect, T arrows represent the inhibition effect and segments show the activation effect or inhibition effect. SXT, Shengxian Decoction; PI3K, phosphoinositide 3-kinase; Akt, protein kinase; LUAD, lung adenocarcinoma.

enriched pathway after the generic cancer pathway, indicating its potential critical role in LUAD treatment (**Figure 9B**).

PPI network construction and analysis of important targets

The PPI network, constructed using STRING for the 197 common targets, is shown in **Figure 10A**. It includes 193 nodes and 2372 edges, with 4 isolated nodes removed. The Cytoscape 3.9.0 platform was used to visualize the PPI networks. Significant targets were identified using CytoNCA based on their DC, CC, and BC values, with thresholds set at $DC \geq 19$, $CC \geq 0.48$, and $BC \geq 58.36$, resulting in a total of 72 important targets. The DC value, indicative of the number of connections to a node, highlights the importance of a node within the network. The top 13 targets, having the highest degrees, were identified as key targets for SXT in LUAD treatment, underlining their critical role in the network (**Figure 10B**; [Supplementary Table 3](#)). **Table 2** shows the 13 key targets and their specific values for DC, CC, and BC were also presented.

Validation of key targets in different databases

To elucidate the possible therapeutic significance and prognostic value of these 13 key targets, their mRNA expression was analysed. The results showed that the mRNA levels of steroid receptor coactivator (SRC), heat shock protein 90 alpha family class A member 1 (HSP90AA1), caspase-3 (CASP3), matrix metalloproteinase-9 (MMP9) and harvey rat sarcoma viral oncogene homolog (HRAS) were significantly higher in LUAD than in normal lung tissues. In contrast, EGFR, estrogen receptor 1 (ESR1), ras homolog gene family, member A (RHOA), MAPK1 and annexin A5 (ANXA5) mRNA expression levels were significantly decreased (**Figure 11A**). Next, we investigated the correlation between the mRNA levels of 13 key targets and different cancer stages of LUAD in the UALCAN database. As shown in **Figure 11B**,

when compared with normal lung tissues, the mRNA levels of SRC, HSP90AA1, CASP3 and MMP9 were increased significantly in stages one to four LUAD tissues, while the expression levels of RHOA and ANXA5 were decreased significantly. For EGFR levels, there was a significant decrease in stage one to three LUAD tissue, but no significant change in stage four. Furthermore, the mRNA expression of serine/threonine protein kinase 1 (AKT1) and insulin like growth factor 1 (IGF1) in different tumor stages had different degrees of expression than that in normal lung tissues, but the difference was not significant.

We further studied the expression levels of 13 key target proteins in LUAD. As shown in **Figure 12**, compared with normal lung tissues, the expression levels of EGFR, SRC, HSP90AA1, CASP3, HRAS, ESR1, IGF1, MAPK1 and ANXA5 were increased in LUAD tissues, while the expression levels of albumin (ALB) and RHOA were decreased in LUAD tissues. These results demonstrated that multiple key targets were abnormally expressed at the protein level in LUAD patients. **Figure 13** shows the impact of 13 key target expressions on the OS rate of LUAD patients. Results indicated that low expression of ALB and AKT1 and high expression of EGFR and HSP90AA1 were closely connected with a poor survival prognosis. We next analyzed the frequency and types of gene changes in 13 key targets in 507 LUAD patients. As shown in **Figure 14**, the overall alteration rate of 13 key targets was 32.94% (167/507) including gene mutation, gene amplification, deep deletion and multiple alterations. The rate of genetic alteration rate of individual genes varied was highest for EGFR (16%) and lowest for ANXA5 (0.8%).

Molecular docking validation

Validation including mRNA and protein expression, survival analysis, and genetic alterations, verified modulation of key targets. Subsequent molecular docking assessed the binding affini-

Potential mechanism of Shengxian Decoction against lung adenocarcinoma

Figure 10. PPI network to demonstrate SXT active component targets for LUAD treatment. A. PPI network diagram of common targets; B. The PPI network diagram of important targets above the median of degree centrality, closeness centrality and betweenness centrality, with the center and first circle representing the key targets. PPI, protein-protein interaction; SXT, Shengxian Decoction; LUAD, lung adenocarcinoma.

Table 2. Ranking of key targets degree

No.	Target	DC	CC	BC
1	ALB	118	0.72	5615.69
2	AKT1	111	0.70	2916.85
3	EGFR	98	0.66	2002.56
4	SRC	87	0.63	1008.92
5	HSP90AA1	85	0.63	1505.92
6	CASP3	85	0.64	1347.02
7	MMP9	83	0.63	1548.34
8	HRAS	81	0.62	1040.10
9	ESR1	79	0.61	1281.94
10	IGF1	77	0.61	721.80
11	RHOA	68	0.58	593.45
12	MAPK1	67	0.58	817.36
13	ANXA5	61	0.58	250.16

Note: Degree centrality (DC) represents the number of links to the node; closeness centrality (CC) represents the distance between the individuals and all other peers in a network; betweenness centrality (BC) is used to measure how often a node lies on the shortest path between nodes in the network. ALB, albumin; AKT1, serine/threonine protein kinase 1; EGFR, epidermal growth factor receptor; SRC, steroid receptor coactivator; HSP90AA1, heat shock protein 90 alpha family class A member 1; CASP3, caspase-3; MMP9, matrix metallo-proteinase-9; HRAS, harvey rat sarcoma viral oncogene homolog; ESR1, estrogen receptor 1; IGF1, insulin like growth factor 1; RHOA, ras homolog gene family member A; MAPK1, mitogen-activated protein kinase 1; ANXA5, annexin A5.

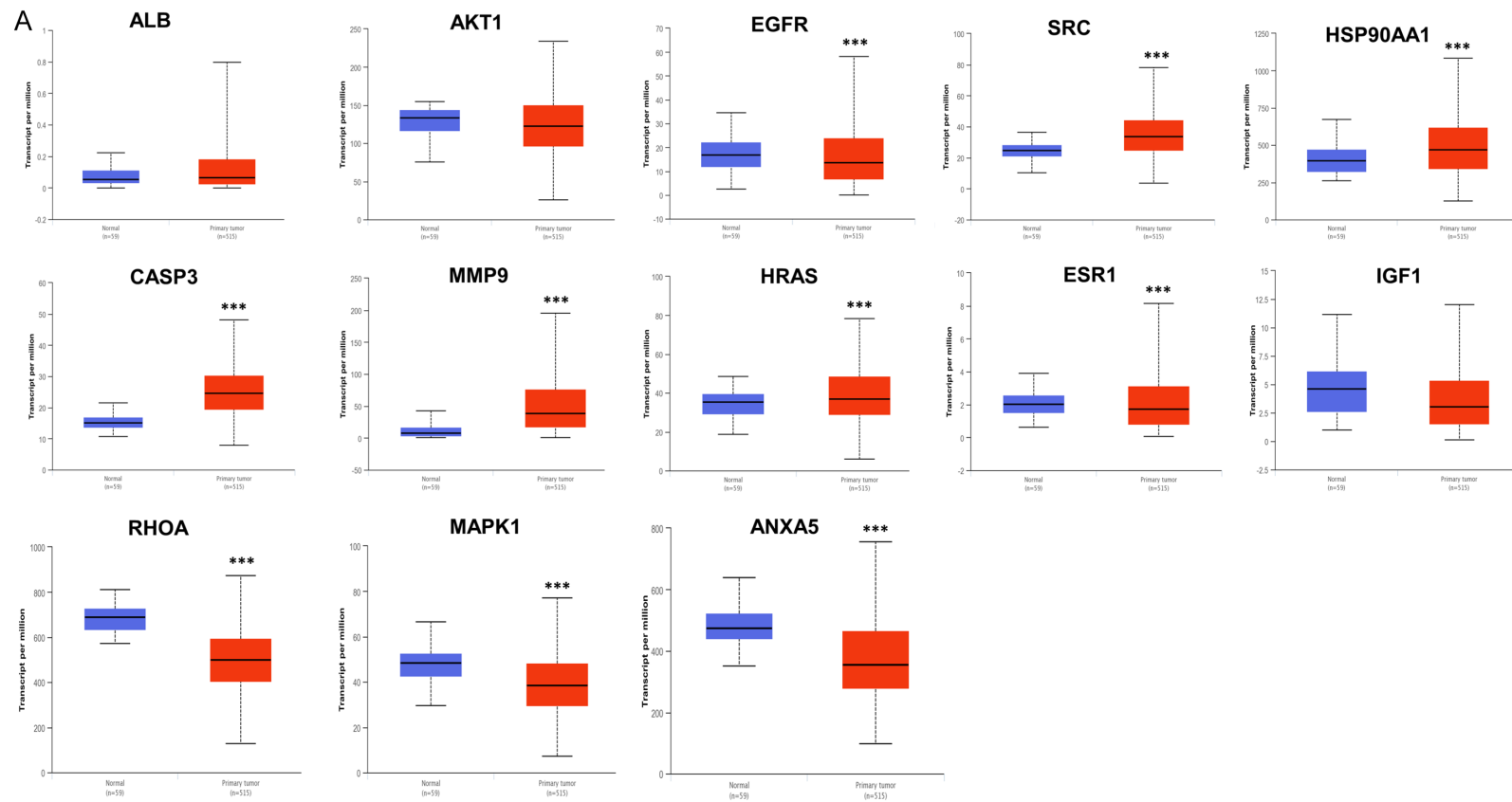
ties of SXT active components to these key targets. The binding energies between SXT active components and the 13 key targets were all below $-5.0 \text{ kJ}\cdot\text{mol}^{-1}$, demonstrating good ligand-receptor interactions (**Figure 15**; [Supplementary Table 4](#)). KEGG pathway analysis revealed that SXT active components inhibits LUAD primarily by modulating the PI3K-Akt signaling pathway, with AKT1 being a pivotal target in apoptosis regulation within this pathway. External database analysis identified EGFR as playing a significant role in LUAD progression and exhibiting the highest degree of variation. These findings align with the PPI results, suggesting that AKT1 and EGFR are critical targets of SXT active components in LUAD treatment. We visualized the top two tar-

gets with the lowest binding energy to AKT1 and EGFR from SXT active components by PyMol, respectively. As shown in **Table 3** and **Figure 16**, neomangiferin and calycosin 7-O-glucoside bind well to the AKT1 active pocket, showing high binding affinities, both with a binding energy of $-10.7 \text{ kJ}\cdot\text{mol}^{-1}$. Neomangiferin binds well to the AKT1 active pocket by binding to amino acid residues glutamic acid (GLU)-85, arginine (ARG)-273, threonine (THR)-82, aspartic acid (ASP)-292, isoleucine (ILE)-290 and THR-211. Calycosin 7-O-glucoside was bound to AKT1 by 5 hydrogen bonds to amino acid residues serine (SER)-205, lysine (LYS)-268, ARG-273, cysteine (CYS)-296 and GLU-298. Neomangiferin and luteolin bind well to EGFR with binding energies of $-9.1 \text{ kJ}\cdot\text{mol}^{-1}$ and $-8.7 \text{ kJ}\cdot\text{mol}^{-1}$, respectively. Neomangiferin binds to EGFR through binding to amino acid residues ARG-841, asparagine (ASN)-842, LYS-745 and proline (PRO)-794. Luteolin binds to EGFR through binding to amino acid residues methionine (MET)-793 and LYS-745. The docking junction results suggest that the SXT active components may be a potential inhibitor for the treatment of LUAD and that the AKT1 and EGFR play a critical role.

Discussion

Current treatment strategies for LUAD typically involve surgery, chemotherapy, radiotherapy, targeted therapy, immunotherapy, or a combination thereof [24]. However, these conventional therapies often result in severe side effects, which can hinder the successful completion of effective radiotherapy and chemotherapy cycles for most patients. Consequently, the search for effective drugs with fewer side effects for LUAD treatment has become a critical area of research. SXT, a commonly used TCM formula, has been clinically applied to treat various diseases, including chronic heart failure and industrial pneumoconiosis [25, 26]. Our prior research demonstrated the effectiveness of SXT in inhibiting tumor growth in A549-xenograft nude mice, with low toxicity to visceral tissues. Additionally, a serum pharmacology

Potential mechanism of Shengxian Decoction against lung adenocarcinoma



Potential mechanism of Shengxian Decoction against lung adenocarcinoma

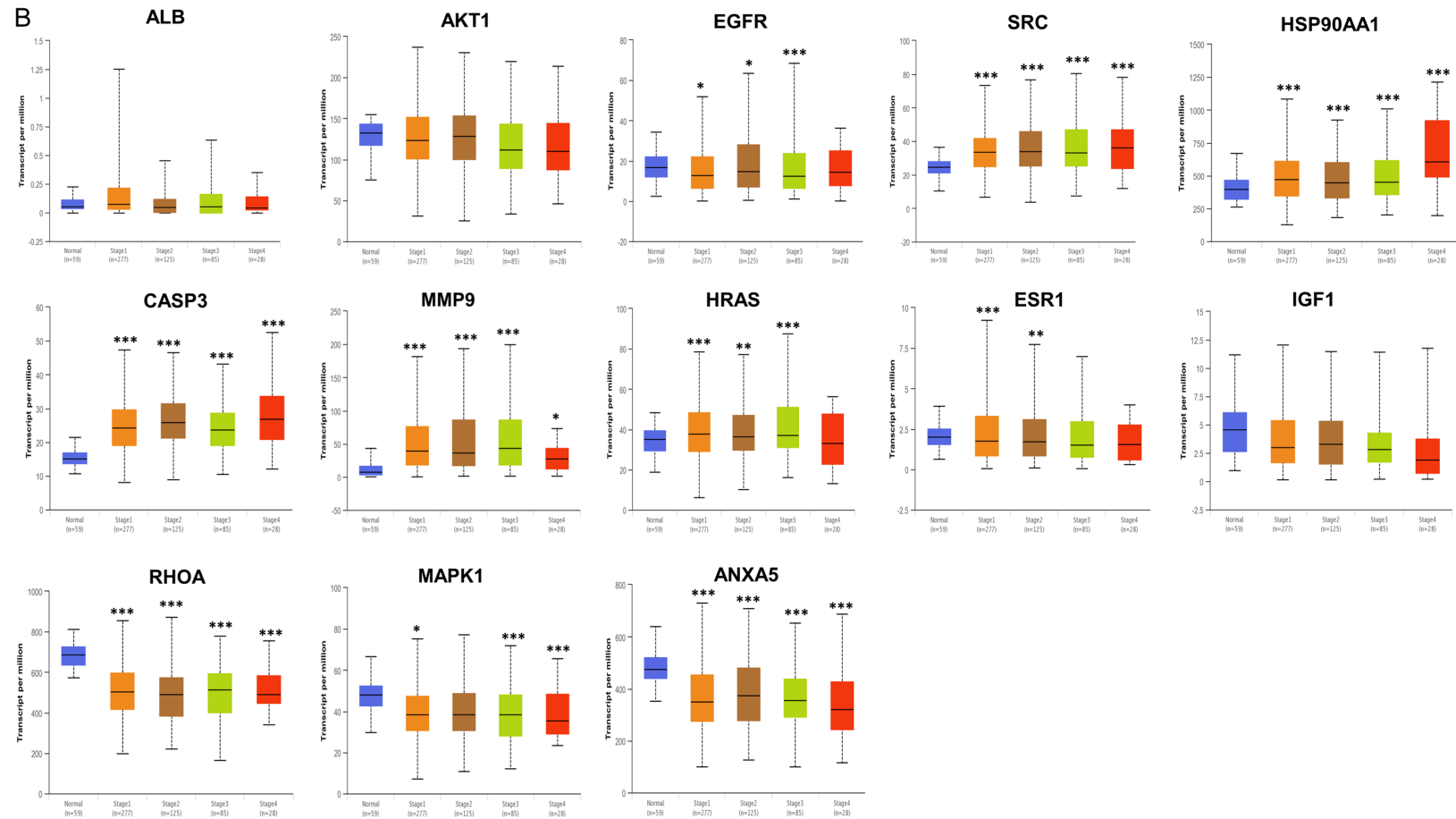


Figure 11. Validation of the mRNA expression of key targets in UALCAN. A. The mRNA levels of 13 key targets in LUAD tissues and normal lung tissues. B. The mRNA levels of 13 key targets in different tumor stages of LUAD (* $P \leq 0.05$, ** $P \leq 0.01$, *** $P \leq 0.001$). LUAD, lung adenocarcinoma; ALB, albumin; AKT1, serine/threonine protein kinase 1; EGFR, epidermal growth factor receptor; SRC, steroid receptor coactivator; HSP90AA1, heat shock protein 90 alpha family class A member 1; CASP3, caspase-3; MMP9, matrix metalloproteinase-9; HRAS, harvey rat sarcoma viral oncogene homolog; ESR1, estrogen receptor 1; IGF1, insulin like growth factor 1; RHOA, ras homolog gene family member A; MAPK1, mitogen-activated protein kinase 1; ANXA5, annexin A5.

Potential mechanism of Shengxian Decoction: against lung adenocarcinoma

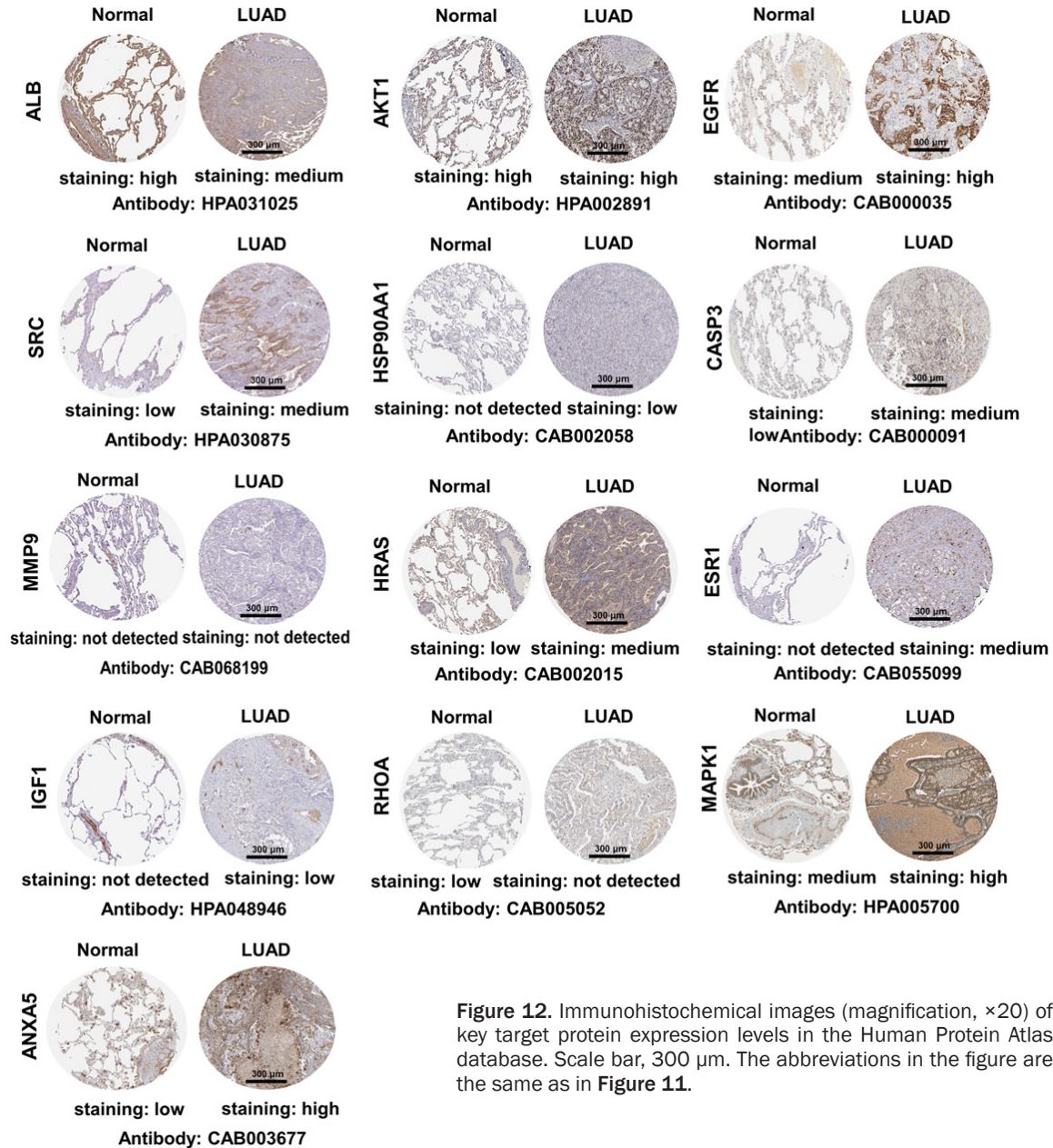


Figure 12. Immunohistochemical images (magnification, $\times 20$) of key target protein expression levels in the Human Protein Atlas database. Scale bar, 300 μm . The abbreviations in the figure are the same as in Figure 11.

assay confirmed the efficacy of SXT-containing serum in inhibiting the growth of three types of LUAD cells (A549, NCI-H1975, and SK-LU-1) in vitro [15]. In this study, we further established that SXT extract significantly inhibited proliferation, migration, and invasion in human LUAD cells (A549 and NCI-H1299) in vitro. These findings encouraged us to further study the active components in SXT extract.

Previous studies have identified mangiferin, neomangiferin, calycosin 7-O-glucoside, formo-

netin, saikosaponin A and isoferulic acid in SXT extract [15, 27]. This study marks the first identification of luteolin in SXT extract. Among these components, neomangiferin can partially convert to mangiferin during the decoction process. Mangiferin has shown anti-tumor properties in A549 xenograft mice and may affect LUAD cells proliferation, cell cycle progression, and apoptosis induction through down-regulating miR-92a and miR-27b expression levels [28]. Calycosin 7-O-glucoside and isoferulic acid also exhibit tumor-suppressive effects by

Potential mechanism of Shengxian Decoction against lung adenocarcinoma

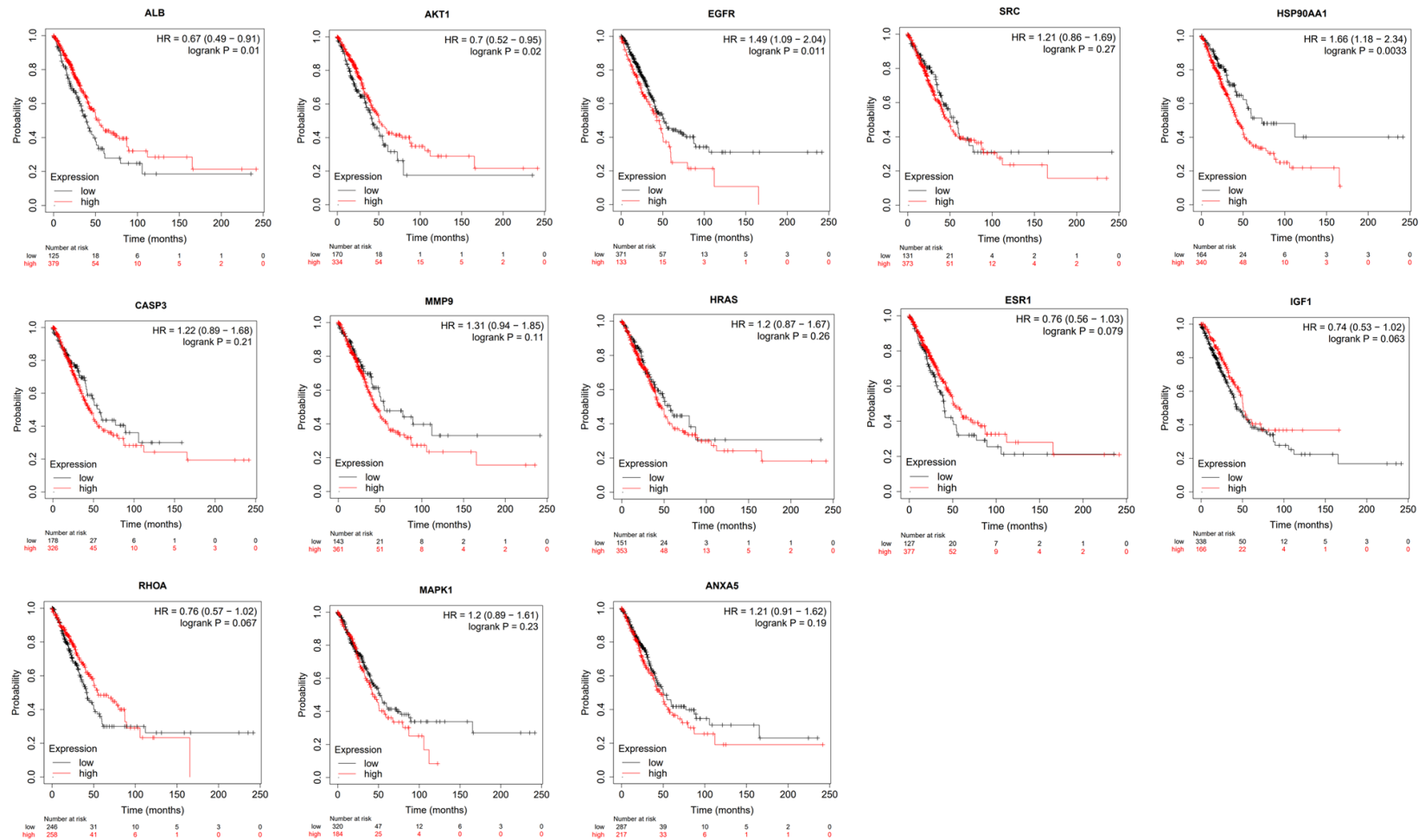


Figure 13. Overall survival analysis of 13 key targets in LUAD in Kaplan-Meier mapper database. * $P \leq 0.05$, ** $P \leq 0.01$. HR, hazard ratio. Other abbreviations in the figure are the same as in Figure 11.

Potential mechanism of Shengxian Decoction against lung adenocarcinoma

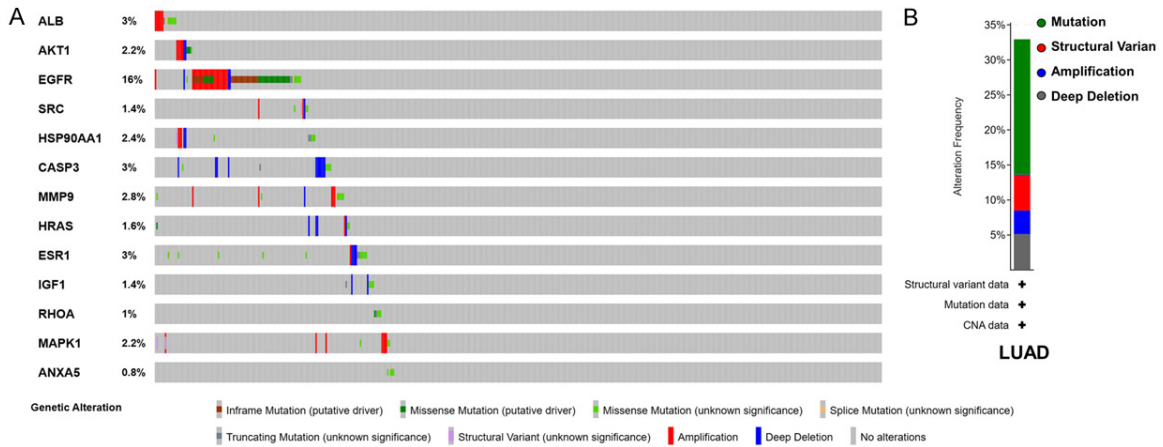


Figure 14. Genetic alterations in 13 key targets in LUAD patients in cBioPortal. A. OncoPrint visual summary of genetic alterations detected in 13 key targets. B. Summary of alterations in 13 key targets in LUAD. The abbreviations in the figure are the same as in **Figure 11**.

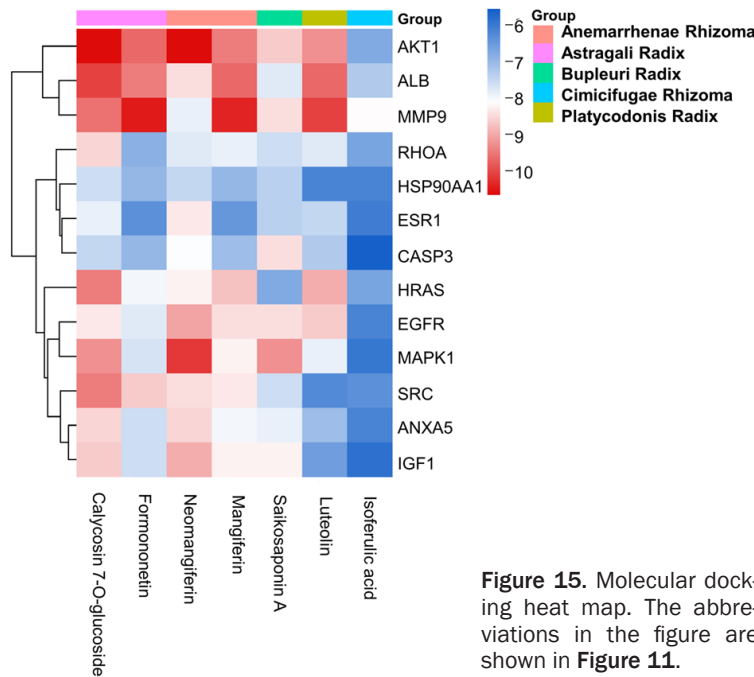


Figure 15. Molecular docking heat map. The abbreviations in the figure are shown in **Figure 11**.

impacting the cell cycle [29, 30]. Formononetin inhibits tumor growth by targeting the EGFR-Akt-myeloid cell leukemia-1 (Mcl-1) axis in NSCLC [31]. Saikosaponin A inhibits migration and invasion of triple-negative breast cancer cells by down-regulating C-X-C chemokine receptor type (CXCR4) expression, inactivating the Akt-mammalian target of rapamycin (mTOR) signaling pathway, and suppressing MMP-9 and MMP-2 expression [32]. Luteolin attenuates lung cancer cell migration and invasion by

inhibiting the focal adhesion kinase and non-receptor tyrosine kinase signaling pathways [33]. To better understand the therapeutic contribution of these active components to LUAD, the chemical composition of SXT extract was identified and quantified. The results showed that SXT extract is particularly rich in saikosaponin A (6.47 mg/g) and mangiferin (3.53 mg/g), which may contribute significantly to the tumor suppression activity of SXT extract.

By integrating data from various databases, 197 targets with therapeutic potential for LUAD treatment by SXT active components were identified. GO analysis indicated that SXT

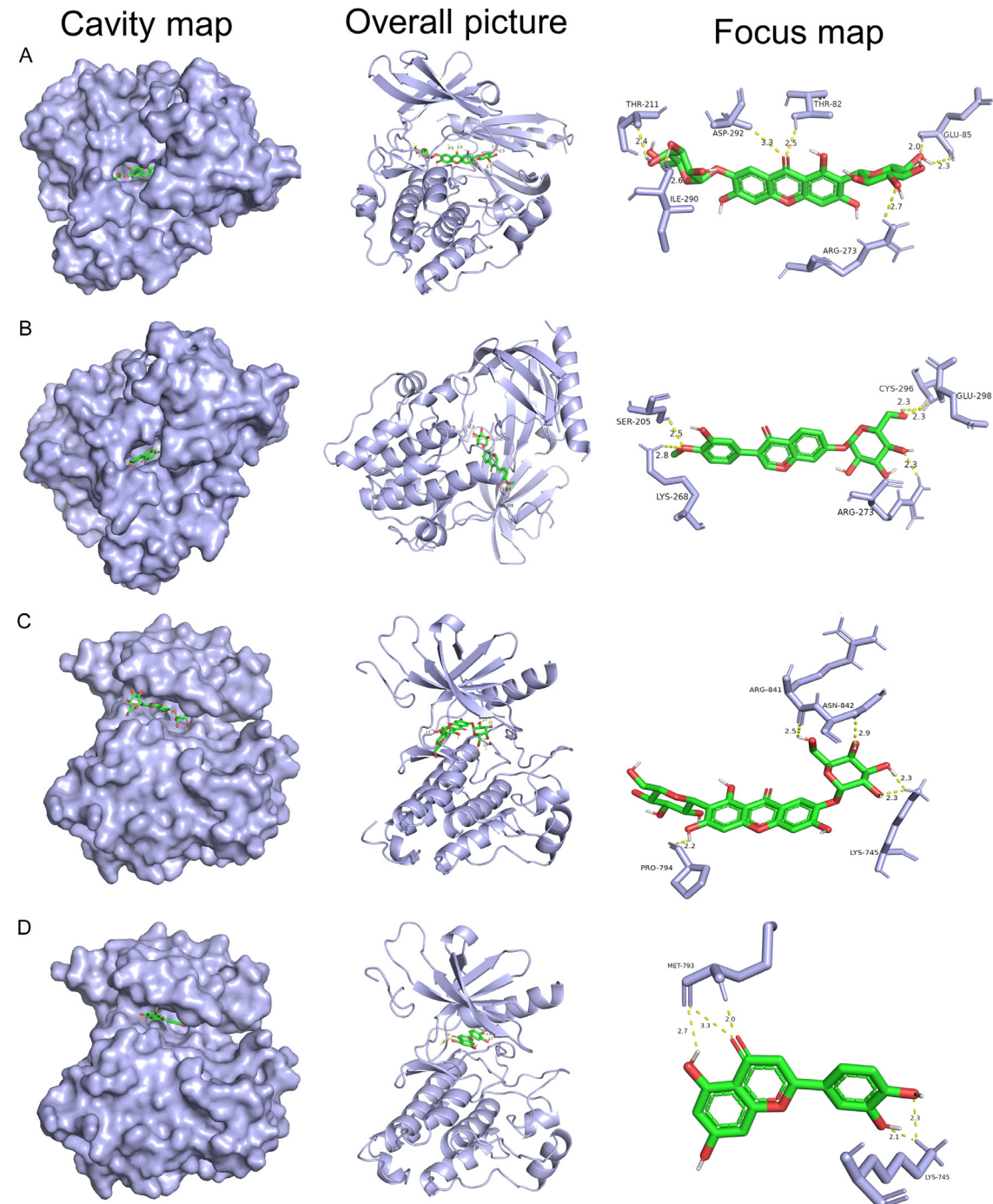
active components could intervene in LUAD progression through biological processes such as apoptosis and protein phosphorylation. KEGG analysis suggested that SXT active components might exert its therapeutic effects on LUAD by regulating pathways like PI3K-Akt, FOXO, and MAPK, all of which have been implicated in lung cancer [34, 35]. The constructed SXT-active components-target-pathway network highlighted the significance of the PI3K-Akt pathway, with key targets (including AKT1,

Potential mechanism of Shengxian Decoction against lung adenocarcinoma

Table 3. Protein, ligand, hydrogen bond and binding energy in molecular docking

Protein	PDB ID	Compounds	H-bond	Binding energy/(kJ·mol ⁻¹)
AKT1	3O96	Neomangiferin	GLU-85, ARG-273, THR-82, ASP-292, ILE-290, THR-211	-10.7
AKT1	3O96	Calycosin 7-O-glucoside	SER-205, LYS-268, ARG-273, CYS-296 GLU-298	-10.7
EGFR	7KXZ	Neomangiferin	ARG-841, ASN-842, LYS-745, PRO-794	-9.1
EGFR	7KXZ	Luteolin	MET-793, LYS-745	-8.7

Note: AKT1, serine/threonine protein kinase 1; EGFR, epidermal growth factor receptor; GLU, glutamic acid; ARG, arginine; THR, threonine; ASP, aspartic acid; ILE, isoleucine; SER, serine; LYS, lysine; CYS, cysteine; ASN, asparagine; PRO, proline; MET, methionine.



Potential mechanism of Shengxian Decoction against lung adenocarcinoma

Figure 16. The picture of molecule docking model of (A) Neomangiferin with AKT1, (B) Calycosin 7-O-glucoside with AKT1, (C) Neomangiferin with EGFR, and (D) Luteolin with EGFR. The green model represents the SXT active components, and the grey model indicates the key target proteins. The hydrogen bonds were represented by yellow dotted lines, and the length was marked around the lines. AKT1, serine/threonine protein kinase 1; EGFR, epidermal growth factor receptor; SXT, Shengxian Decoction; GLU, glutamic acid; ARG, arginine; THR, threonine; ASP, aspartic acid; ILE, isoleucine; SER, serine; LYS, lysine; CYS, cysteine; ASN, asparagine; PRO, proline; MET, methionine.

EGFR, HSP90AA1, HRAS, IGF1, MAPK3, and MAPK1) predominantly enriched in this pathway. The PI3K-Akt pathway is crucial for regulating various processes, including cell proliferation, apoptosis, necrosis, and inflammation [36]. The EGFR signaling pathway, critical in tumor progression, activates the PI3K-Akt pathways, leading to cell proliferation, invasion, and migration [37]. The EGFR-MAPK pathway is activated in LUAD to promote tumor growth and metastasis [38], while FOXO signaling pathways are triggered by PI3K-Akt, mediating cellular functions related to proliferation and growth [39]. Considering the inhibition of tumor cell proliferation and promotion of apoptosis as viable cancer treatment pathways, this study preliminarily infers that SXT active components could potentially inhibit LUAD by targeting pathways related to cell proliferation and apoptosis.

The 13 key targets with top-degree values may play a critical role in treating LUAD, which were then validated in different databases. EGFR is a determinant that drives the growth and in vivo therapeutic response of LUAD [40]. AKT1 is a key metastasis regulator in LUAD cells and that inhibition of AKT1 promoted migration and invasion of KRAS or EGFR mutated LUAD cells in vitro [41]. SRC promotes the metastasis of various tumors, including NSCLC. Moreover, SRC can be used as an anti-cancer molecular target, and inhibition of SRC can inhibit multiple signaling pathways, including the EGFR pathway [42]. The knockdown of HSP90AA1 is able to inhibit AKT1 expression, thus inhibiting lung cancer cell proliferation [43]. CASP3 plays a central role in executing apoptosis and is involved in carcinogenesis [44]. In addition, analysis of the UALCAN database with the HPA database showed that the mRNA and protein levels of EGFR, SRC, HSP90AA1 and CASP3 were significantly altered in LUAD tissues, which may contribute to the occurrence of LUAD. Based on the Kaplan-Meier mapper database, high expression of EGFR and HSP90AA1, as

well as low expression of AKT1, were associated with significant poor survival. The cBioPortal database shows that the mutation rate of EGFR in LUAD is as high as 16%, suggesting that EGFR has an important role in LUAD progression. The above studies indicate that SXT active components can regulate the expression of key targets and inhibit the malignant biological behaviors such as proliferation, migration, and invasive ability of LUAD cells, and thus can be used for the LUAD treatment.

Finally, we verified the binding affinities of compounds to the targets using molecular docking techniques. For instance, neomangiferin bound to AKT1 by forming hydrogen bonds with amino acid residues THR-82 and THR-211 ($-10.7 \text{ kJ}\cdot\text{mol}^{-1}$). It was further speculated whether the active binding of neomangiferin to AKT1 could lead to abnormal phosphorylation at threonine residues in the active pocket of ATP and thus contribute to the treatment of LUAD. Luteolin demonstrated strong binding affinity to the ATP-binding pocket of EGFR ($-8.7 \text{ kJ}\cdot\text{mol}^{-1}$), and formed a hydrogen bond with the backbone nitrogen of Met793. This interaction between EGFR and Luteolin may disrupt the interaction between EGFR and ATP, thereby inhibiting the activation of downstream signaling pathways, such as the EGFR-PI3K-Akt pathway, closely related to proliferation and apoptosis. The interaction of multiple active components in SXT extract with this pathway suggests that SXT treats LUAD through a multifaceted approach involving multiple components and targets (**Figure 17**).

Conclusion

In summary, this study demonstrated the inhibitory activity of SXT extract on LUAD cells in vitro and identified the main bioactive components using HPLC. Furthermore, the potential mechanisms of SXT in LUAD treatment were elucidated through network pharmacology, external validation databases, and molecular docking. It is postulated that SXT may impede

Potential mechanism of Shengxian Decoction against lung adenocarcinoma

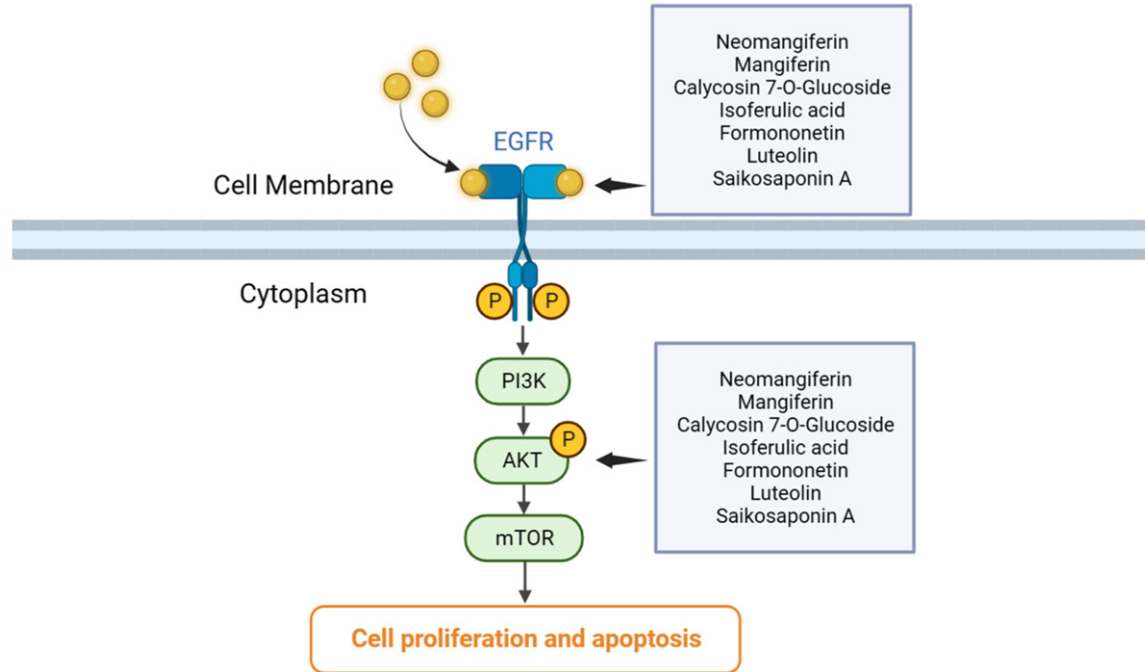


Figure 17. Schematic representation of the multi-component and multi-target of SXT intervening in the development of lung adenocarcinoma. SXT, Shengxian Decoction; EGFR, epidermal growth factor receptor; PI3K, phosphoinositide 3-kinase; AKT, serine/threonine protein kinase; mTOR, mammalian target of rapamycin.

LUAD proliferation, migration, and invasion by facilitating interactions between its main active components, such as saikosaponin A and mangiferin, with 13 key targets, including ALB, AKT1, EGFR, and SRC, through EGFR-PI3K-Akt and other signaling pathways. This study provides a theoretical foundation for further investigation and application of SXT in the treatment of LUAD.

Acknowledgements

K. Li thanks the support from the Natural Science Foundation of Sichuan Province (22NSFSC1268) and the National Natural Science Foundation of China (81904081). F. You is grateful to the Science and Technology Major Project of Sichuan Province of China (2022ZDZX0022) and the Central Guidance on Local Science and Technology Development Fund of Sichuan Province of China (2022ZYD0100).

Disclosure of conflict of interest

None.

Address correspondence to: Dr. Kejuan Li, College of Life Science, Sichuan Normal University, No. 5,

Jing'an Road, Jinjiang District, Chengdu 610066, Sichuan, China. E-mail: likejuan@sicnu.edu.cn; Dr. Fengming You, Traditional Chinese Medicine (TCM) Regulating Metabolic Diseases Key Laboratory of Sichuan Province, Hospital of Chengdu University of Traditional Chinese Medicine, No. 37, Shier Qiao Road, Jinniu District, Chengdu 610075, Sichuan, China. E-mail: yfmdoc@163.com

References

- [1] Hirsch FR, Scagliotti GV, Mulshine JL, Kwon R, Curran WJ Jr, Wu YL and Paz-Ares L. Lung cancer: current therapies and new targeted treatments. *Lancet* 2017; 389: 299-311.
- [2] Ferlay J, Soerjomataram I, Dikshit R, Eser S, Mathers C, Rebelo M, Parkin DM, Forman D and Bray F. Cancer incidence and mortality worldwide: sources, methods and major patterns in GLOBOCAN 2012. *Int J Cancer* 2015; 136: E359-386.
- [3] Sun D, Li H, Cao M, He S, Lei L, Peng J and Chen W. Cancer burden in China: trends, risk factors and prevention. *Cancer Biol Med* 2020; 17: 879-895.
- [4] Zhou XJ, Li R, Liu X and Qu YQ. Advances in deubiquitinating enzymes in lung adenocarcinoma. *J Cancer* 2021; 12: 5573-5582.
- [5] Li ZH, Yu D, Huang NN, Wu JK, Du XW and Wang XJ. Immunoregulatory mechanism stud-

Potential mechanism of Shengxian Decoction against lung adenocarcinoma

- ies of ginseng leaves on lung cancer based on network pharmacology and molecular docking. *Sci Rep* 2021; 11: 18201.
- [6] Zhang W, Tian W, Wang Y, Jin X, Guo H, Wang Y, Tang Y and Yao X. Explore the mechanism and substance basis of Mahuang FuziXixin Decoction for the treatment of lung cancer based on network pharmacology and molecular docking. *Comput Biol Med* 2022; 151: 106293.
- [7] Wang ZY, Li MZ, Li WJ, Ouyang JF, Gou XJ and Huang Y. Mechanism of action of Daqinjiao decoction in treating cerebral small vessel disease explored using network pharmacology and molecular docking technology. *Phytomedicine* 2023; 108: 154538.
- [8] Li Q, Liu P, Wu C, Bai L, Zhang Z, Bao Z, Zou M, Ren Z, Yuan L, Liao M, Lan Z, Yin S and Chen L. Integrating network pharmacology and pharmacological validation to explore the effect of Shi Wei Ru Xiang powder on suppressing hyperuricemia. *J Ethnopharmacol* 2022; 298: 115679.
- [9] Huang C, Qiu S, Fan X, Jiao G, Zhou X, Sun M, Weng N, Gao S, Tao X, Zhang F and Chen W. Evaluation of the effect of Shengxian Decoction on doxorubicin-induced chronic heart failure model rats and a multicomponent comparative pharmacokinetic study after oral administration in normal and model rats. *Biomed Pharmacother* 2021; 144: 112354.
- [10] He H, Zhou X, Wang Q and Zhao Y. Does the cause of astragalus-containing Chinese herbal prescriptions and radiotherapy benefit to non-small-cell lung cancer treatment: a meta-analysis of randomized trials. *Evid Based Complement Alternat Med* 2013; 2013: 426207.
- [11] Wang Q, Zheng XL, Yang L, Shi F, Gao LB, Zhong YJ, Sun H, He F, Lin Y and Wang X. Reactive oxygen species-mediated apoptosis contributes to chemosensitization effect of saikosaponins on cisplatin-induced cytotoxicity in cancer cells. *J Exp Clin Cancer Res* 2010; 29: 159.
- [12] Zhou C, Yu T, Zhu R, Lu J, Ouyang X, Zhang Z, Chen Q, Li J, Cui J, Jiang F, Jin KY, Sarapultsev A, Li F, Zhang G, Luo S and Hu D. Timosaponin AIII promotes non-small-cell lung cancer ferroptosis through targeting and facilitating HSP90 mediated GPX4 ubiquitination and degradation. *Int J Biol Sci* 2023; 19: 1471-1489.
- [13] Jeong SH, Guo H, Kim HY and Park JB. Ethanol extract of *Cimicifugae* rhizoma exerted more potent anti-inflammatory and tumor suppressor activities compared with methanol and water extracts. *Biomed Res India* 2016; 27: 1054-1059.
- [14] Shen HS and Wen SH. Effect of early use of Chinese herbal products on mortality rate in patients with lung cancer. *J Ethnopharmacol* 2018; 211: 1-8.
- [15] Li K, You F, Zhang Q, Yuan R, Yuan Q, Fu X, Ren Y, Wang Q, Li X, Zhang Z, Shichiri M and Yu Y. Chemical and biological evidence of the efficacy of Shengxian Decoction for treating human lung adenocarcinoma. *Front Oncol* 2022; 12: 849579.
- [16] Liu X, Ouyang S, Yu B, Liu Y, Huang K, Gong J, Zheng S, Li Z, Li H and Jiang H. PharmMapper server: a web server for potential drug target identification using pharmacophore mapping approach. *Nucleic Acids Res* 2010; 38: W609-614.
- [17] Wang X, Pan C, Gong J, Liu X and Li H. Enhancing the enrichment of pharmacophore-based target prediction for the polypharmacological profiles of drugs. *J Chem Inf Model* 2016; 56: 1175-1183.
- [18] Wang X, Shen Y, Wang S, Li S, Zhang W, Liu X, Lai L, Pei J and Li H. PharmMapper 2017 update: a web server for potential drug target identification with a comprehensive target pharmacophore database. *Nucleic Acids Res* 2017; 45: W356-W360.
- [19] Zhang Y, Li Z, Yang M, Wang D, Yu L, Guo C, Guo X and Lin N. Identification of GRB2 and GAB1 coexpression as an unfavorable prognostic factor for hepatocellular carcinoma by a combination of expression profile and network analysis. *PLoS One* 2013; 8: e85170.
- [20] Chandrashekar DS, Karthikeyan SK, Korla PK, Patel H, Shovon AR, Athar M, Netto GJ, Qin ZS, Kumar S, Manne U, Creighton CJ and Varambally S. UALCAN: an update to the integrated cancer data analysis platform. *Neoplasia* 2022; 25: 18-27.
- [21] Chandrashekar DS, Bashel B, Balasubramanya SAH, Creighton CJ, Ponce-Rodriguez I, Chakravarthi BVSK and Varambally S. UALCAN: a portal for facilitating tumor subgroup gene expression and survival analyses. *Neoplasia* 2017; 19: 649-658.
- [22] Uhlén M, Fagerberg L, Hallström BM, Lindskog C, Oksvold P, Mardinoglu A, Sivertsson Å, Kampf C, Sjöstedt E, Asplund A, Olsson I, Edlund K, Lundberg E, Navani S, Szigartyo CA, Odeberg J, Djureinovic D, Takanen JO, Hober S, Alm T, Edqvist PH, Berling H, Tegel H, Mulder J, Rockberg J, Nilsson P, Schwenk JM, Hamsten M, von Feilitzen K, Forsberg M, Persson L, Johansson F, Zwahlen M, von Heijne G, Nielsen J and Pontén F. Proteomics. Tissue-based map of the human proteome. *Science* 2015; 347: 1260419.
- [23] Lánckzy A and Györfy B. Web-based survival analysis tool tailored for medical research (KMplot): development and implementation. *J Med Internet Res* 2021; 23: e27633.
- [24] Kim W, Lee WB, Lee JW, Min BI, Baek SK, Lee HS and Cho SH. Traditional herbal medicine as adjunctive therapy for breast cancer: a system-

Potential mechanism of Shengxian Decoction against lung adenocarcinoma

- atic review. *Complement Ther Med* 2015; 23: 626-632.
- [25] Ma Y, Wang BL, Wang L, Huang CY, Sun M, Jiao GY, Zhang F and Chen WS. Effective components of Shengxian Decoction and its mechanism of action in treating chronic heart failure based on UHPLC-Q-TOF-MS integrated with network pharmacology. *Zhongguo Zhong Yao Za Zhi* 2021; 46: 2489-2500.
- [26] Wang HJ and Ma GQ. Introduction to Professor Ma Guiqin's experience in treatment of occupational pneumoconiosis. *Zhongguo Zhong Yao Za Zhi* 2019; 44: 2871-2874.
- [27] Wang M, Li H, Gao Y, Li Y, Sun Y, Liu S and Liu Z. A multidimensional strategy to rapidly identify the chemical constituents in Shengxian Decoction by using ultra-performance liquid chromatography coupled with ion mobility spectrometry quadrupole time-of-flight mass spectrometry. *J Sep Sci* 2022; 45: 3115-3127.
- [28] Chi XJ, Meng JJ, Lin CY, Su QS, Qin YY, Wei RH, Lan D and Huang C. Mangiferin inhibits human lung adenocarcinoma by suppressing miR-27b and miR-92a. *Evid Based Complement Alternat Med* 2021; 2021: 2822950.
- [29] Bratkov VM, Shkondrov AM, Zdraveva PK and Krasteva IN. Flavonoids from the genus astragalus: phytochemistry and biological activity. *Pharmacogn Rev* 2016; 10: 11-32.
- [30] Long Z, Feng G, Zhao N, Wu L and Zhu H. Isoferulic acid inhibits human leukemia cell growth through induction of G2/M-phase arrest and inhibition of Akt/mTOR signaling. *Mol Med Rep* 2020; 21: 1035-1042.
- [31] Yu X, Gao F, Li W, Zhou L, Liu W and Li M. Formononetin inhibits tumor growth by suppression of EGFR-Akt-Mcl-1 axis in non-small cell lung cancer. *J Exp Clin Cancer Res* 2020; 39: 62.
- [32] Wang Y, Zhao L, Han X, Wang Y, Mi J, Wang C, Sun D, Fu Y, Zhao X, Guo H and Wang Q. Saikosaponin A inhibits triple-negative breast cancer growth and metastasis through downregulation of CXCR4. *Front Oncol* 2020; 9: 1487.
- [33] Masraksa W, Tanasawet S, Hutamekalin P, Wongtawatchai T and Sukketsiri W. Luteolin attenuates migration and invasion of lung cancer cells via suppressing focal adhesion kinase and non-receptor tyrosine kinase signaling pathway. *Nutr Res Pract* 2020; 14: 127-133.
- [34] Hao P, Huang Y, Peng J, Yu J, Guo X, Bao F, Dian Z, An S and Xu TR. IRS4 promotes the progression of non-small cell lung cancer and confers resistance to EGFR-TKI through the activation of PI3K/Akt and Ras-MAPK pathways. *Exp Cell Res* 2021; 403: 112615.
- [35] Sun T, Zhang J, Deng B, Fan X, Long T, Jin H, Tao S, Kang P and Tan Q. FOXO1 and FOXO3a sensitize non-small-cell lung cancer cells to cisplatin-induced apoptosis independent of Bim. *Acta Biochim Biophys Sin (Shanghai)* 2020; 52: 1348-1359.
- [36] Iksen, Pothongsrisit S and Pongrakhananon V. Targeting the PI3K/AKT/mTOR signaling pathway in lung cancer: an update regarding potential drugs and natural products. *Molecules* 2021; 26: 4100.
- [37] Jiang J, Yuan Z, Sun Y, Bu Y, Li W and Fei Z. Ginsenoside Rg3 enhances the anti-proliferative activity of erlotinib in pancreatic cancer cell lines by downregulation of EGFR/PI3K/Akt signaling pathway. *Biomed Pharmacother* 2017; 96: 619-625.
- [38] Xu H, Yang X, Xuan X, Wu D, Zhang J, Xu X, Zhao Y, Ma C and Li D. STAMBP promotes lung adenocarcinoma metastasis by regulating the EGFR/MAPK signaling pathway. *Neoplasia* 2021; 23: 607-623.
- [39] Farhan M, Wang H, Gaur U, Little PJ, Xu J and Zheng W. FOXO signaling pathways as therapeutic targets in cancer. *Int J Biol Sci* 2017; 13: 815-827.
- [40] Foggetti G, Li C, Cai H, Hellyer JA, Lin WY, Ayeni D, Hastings K, Choi J, Wurtz A, Andrejka L, Maghini DG, Rashleigh N, Levy S, Homer R, Gettinger SN, Diehn M, Wakelee HA, Petrov DA, Winslow MM and Politi K. Genetic determinants of EGFR-driven lung cancer growth and therapeutic response in vivo. *Cancer Discov* 2021; 11: 1736-1753.
- [41] Rao G, Pierobon M, Kim IK, Hsu WH, Deng J, Moon YW, Petricoin EF, Zhang YW, Wang Y and Giaccone G. Inhibition of AKT1 signaling promotes invasion and metastasis of non-small cell lung cancer cells with K-RAS or EGFR mutations. *Sci Rep* 2017; 7: 7066.
- [42] Giaccone G and Zucali PA. Src as a potential therapeutic target in non-small-cell lung cancer. *Ann Oncol* 2008; 19: 1219-1223.
- [43] Niu M, Zhang B, Li L, Su Z, Pu W, Zhao C, Wei L, Lian P, Lu R, Wang R, Wazir J, Gao Q, Song S and Wang H. Targeting HSP90 inhibits proliferation and induces apoptosis through AKT1/ERK pathway in lung cancer. *Front Pharmacol* 2022; 12: 724192.
- [44] Lin J, Zhang Y, Wang H, Chang J, Wei L, Cao L, Zhang Z and Zhang X. Genetic polymorphisms in the apoptosis-associated gene CASP3 and the risk of lung cancer in Chinese population. *PLoS One* 2016; 11: e0164358.

Potential mechanism of Shengxian Decoction against lung adenocarcinoma

Supplementary Table 2. The Kyoto Encyclopedia of Genes and Genomes (KEGG) pathway as a relevant target for Shengxian Decoction treatment of lung adenocarcinoma

	Category	Description	Count	Percent (%)	P value
KEGG pathway	Human Diseases	Pathways in cancer	63	31.98	3.25E-30
KEGG pathway	Human Diseases	Lipid and atherosclerosis	36	18.27	1.58E-21
KEGG pathway	Human Diseases	Prostate cancer	23	11.68	5.40E-17
KEGG pathway	Human Diseases	Proteoglycans in cancer	30	15.23	3.14E-16
KEGG pathway	Human Diseases	Non-small cell lung cancer	18	9.14	1.17E-13
KEGG pathway	Human Diseases	Endocrine resistance	20	10.15	1.84E-13
KEGG pathway	Human Diseases	EGFR tyrosine kinase inhibitor resistance	18	9.14	6.03E-13
KEGG pathway	Human Diseases	Chemical carcinogenesis - reactive oxygen species	27	13.71	1.45E-12
KEGG pathway	Human Diseases	AGE-RAGE signaling pathway in diabetic complications	19	9.64	3.14E-12
KEGG pathway	Human Diseases	Colorectal cancer	17	8.63	3.16E-11
KEGG pathway	Human Diseases	Hepatitis B	22	11.17	3.21E-11
KEGG pathway	Human Diseases	Fluid shear stress and atherosclerosis	20	10.15	1.16E-10
KEGG pathway	Human Diseases	Chemical carcinogenesis - receptor activation	24	12.18	1.40E-10
KEGG pathway	Human Diseases	Gastric cancer	20	10.15	3.95E-10
KEGG pathway	Human Diseases	Hepatocellular carcinoma	21	10.66	4.63E-10
KEGG pathway	Human Diseases	Pancreatic cancer	15	7.61	6.54E-10
KEGG pathway	Human Diseases	Chronic myeloid leukemia	15	7.61	6.54E-10
KEGG pathway	Human Diseases	Bladder cancer	12	6.09	6.62E-10
KEGG pathway	Human Diseases	Acute myeloid leukemia	14	7.11	1.39E-09
KEGG pathway	Human Diseases	Toxoplasmosis	17	8.63	1.91E-09
KEGG pathway	Human Diseases	Central carbon metabolism in cancer	14	7.11	2.46E-09
KEGG pathway	Human Diseases	Central carbon metabolism in cancer	14	7.11	2.46E-09
KEGG pathway	Human Diseases	Melanoma	14	7.11	3.54E-09
KEGG pathway	Human Diseases	Small cell lung cancer	15	7.61	8.86E-09
KEGG pathway	Human Diseases	Breast cancer	18	9.14	1.57E-08
KEGG pathway	Human Diseases	Renal cell carcinoma	13	6.6	2.26E-08
KEGG pathway	Human Diseases	Endometrial cancer	12	6.09	3.46E-08
KEGG pathway	Human Diseases	Platinum drug resistance	13	6.6	4.37E-08
KEGG pathway	Human Diseases	Tuberculosis	19	9.64	5.81E-08
KEGG pathway	Human Diseases	Glioma	13	6.6	5.98E-08
KEGG pathway	Human Diseases	Human cytomegalovirus infection	21	10.66	7.45E-08
KEGG pathway	Human Diseases	Yersinia infection	16	8.12	2.38E-07
KEGG pathway	Human Diseases	Epithelial cell signaling in Helicobacter pylori infection	12	6.09	2.62E-07
KEGG pathway	Human Diseases	Measles	16	8.12	2.89E-07
KEGG pathway	Human Diseases	Diabetic cardiomyopathy	19	9.64	3.62E-07
KEGG pathway	Human Diseases	PD-L1 expression and PD-1 checkpoint pathway in cancer	13	6.6	4.17E-07
KEGG pathway	Human Diseases	Kaposi sarcoma-associated herpesvirus infection	18	9.14	9.20E-07
KEGG pathway	Human Diseases	Choline metabolism in cancer	13	6.6	1.20E-06
KEGG pathway	Human Diseases	Hepatitis C	16	8.12	1.40E-06
KEGG pathway	Human Diseases	Chagas disease	13	6.6	1.86E-06
KEGG pathway	Human Diseases	Human T-cell leukemia virus 1 infection	18	9.14	5.90E-06
KEGG pathway	Human Diseases	Epstein-Barr virus infection	17	8.63	7.30E-06
KEGG pathway	Human Diseases	Transcriptional misregulation in cancer	16	8.12	1.79E-05
KEGG pathway	Human Diseases	Non-alcoholic fatty liver disease	14	7.11	2.97E-05
KEGG pathway	Human Diseases	Viral carcinogenesis	16	8.12	3.46E-05
KEGG pathway	Human Diseases	Shigellosis	17	8.63	8.72E-05
KEGG pathway	Human Diseases	Salmonella infection	17	8.63	9.60E-05
KEGG pathway	Human Diseases	Insulin resistance	11	5.58	1.11E-04
KEGG pathway	Human Diseases	Coronavirus disease - COVID-19	16	8.12	1.49E-04
KEGG pathway	Human Diseases	Human papillomavirus infection	19	9.64	2.90E-04
KEGG pathway	Human Diseases	Influenza A	13	6.6	3.30E-04
KEGG pathway	Human Diseases	Human immunodeficiency virus 1 infection	14	7.11	6.88E-04

Potential mechanism of Shengxian Decoction against lung adenocarcinoma

KEGG pathway	Human Diseases	Chemical carcinogenesis - DNA adducts	8	4.06	6.99E-04
KEGG pathway	Human Diseases	MicroRNAs in cancer	17	8.63	1.11E-03
KEGG pathway	Human Diseases	Thyroid cancer	6	3.05	1.13E-03
KEGG pathway	Human Diseases	Pathogenic Escherichia coli infection	13	6.6	1.17E-03
KEGG pathway	Human Diseases	Pertussis	8	4.06	1.25E-03
KEGG pathway	Human Diseases	Bacterial invasion of epithelial cells	8	4.06	1.35E-03
KEGG pathway	Human Diseases	Legionellosis	7	3.55	1.39E-03
KEGG pathway	Human Diseases	Type II diabetes mellitus	6	3.05	3.03E-03
KEGG pathway	Human Diseases	Alzheimer disease	17	8.63	9.13E-03
KEGG pathway	Metabolism	Drug metabolism - other enzymes	10	5.08	5.37E-05
KEGG pathway	Metabolism	Drug metabolism - cytochrome P450	9	4.57	1.54E-04
KEGG pathway	Metabolism	Metabolism of xenobiotics by cytochrome P450	9	4.57	2.70E-04
KEGG pathway	Metabolism	Glycolysis/Gluconeogenesis	7	3.55	3.20E-03
KEGG pathway	Metabolism	Metabolic pathways	48	24.37	7.02E-03
KEGG pathway	Metabolism	Pyrimidine metabolism	6	3.05	8.24E-03
KEGG pathway	Environmental Information Processing	PI3K-Akt signaling pathway	39	19.8	6.22E-17
KEGG pathway	Environmental Information Processing	FoxO signaling pathway	24	12.18	4.27E-15
KEGG pathway	Environmental Information Processing	MAPK signaling pathway	32	16.24	1.27E-13
KEGG pathway	Environmental Information Processing	Ras signaling pathway	28	14.21	7.34E-13
KEGG pathway	Environmental Information Processing	Rap1 signaling pathway	24	12.18	1.15E-10
KEGG pathway	Environmental Information Processing	VEGF signaling pathway	14	7.11	2.59E-10
KEGG pathway	Environmental Information Processing	ErbB signaling pathway	15	7.61	3.05E-09
KEGG pathway	Environmental Information Processing	HIF-1 signaling pathway	16	8.12	1.06E-08
KEGG pathway	Environmental Information Processing	Phospholipase D signaling pathway	17	8.63	1.11E-07
KEGG pathway	Environmental Information Processing	mTOR signaling pathway	16	8.12	1.29E-06
KEGG pathway	Environmental Information Processing	Sphingolipid signaling pathway	14	7.11	1.61E-06
KEGG pathway	Environmental Information Processing	TNF signaling pathway	13	6.6	5.03E-06
KEGG pathway	Environmental Information Processing	JAK-STAT signaling pathway	13	6.6	2.00E-04
KEGG pathway	Environmental Information Processing	AMPK signaling pathway	11	5.58	2.66E-04
KEGG pathway	Environmental Information Processing	Apelin signaling pathway	10	5.08	3.18E-03
KEGG pathway	Cellular Processes	Focal adhesion	23	11.68	3.06E-10
KEGG pathway	Cellular Processes	Apoptosis	18	9.14	4.76E-09
KEGG pathway	Cellular Processes	Adherens junction	13	6.6	3.16E-08
KEGG pathway	Cellular Processes	Cellular senescence	17	8.63	2.32E-07
KEGG pathway	Cellular Processes	Signaling pathways regulating pluripotency of stem cells	16	8.12	4.19E-07
KEGG pathway	Cellular Processes	Autophagy - animal	14	7.11	1.07E-05
KEGG pathway	Cellular Processes	Apoptosis - multiple species	6	3.05	5.69E-04
KEGG pathway	Cellular Processes	Regulation of actin cytoskeleton	14	7.11	8.85E-04
KEGG pathway	Cellular Processes	Cell cycle	10	5.08	1.63E-03
KEGG pathway	Cellular Processes	Oocyte meiosis	10	5.08	2.13E-03
KEGG pathway	Cellular Processes	Endocytosis	14	7.11	3.14E-03
KEGG pathway	Cellular Processes	p53 signaling pathway	7	3.55	4.91E-03
KEGG pathway	Organismal Systems	Estrogen signaling pathway	22	11.17	1.35E-12
KEGG pathway	Organismal Systems	Prolactin signaling pathway	16	8.12	1.57E-11
KEGG pathway	Organismal Systems	Relaxin signaling pathway	20	10.15	3.06E-11
KEGG pathway	Organismal Systems	C-type lectin receptor signaling pathway	17	8.63	6.18E-10
KEGG pathway	Organismal Systems	Fc epsilon RI signaling pathway	14	7.11	1.69E-09
KEGG pathway	Organismal Systems	Progesterone-mediated oocyte maturation	16	8.12	4.15E-09
KEGG pathway	Organismal Systems	Neurotrophin signaling pathway	17	8.63	4.72E-09
KEGG pathway	Organismal Systems	T cell receptor signaling pathway	16	8.12	5.47E-09
KEGG pathway	Organismal Systems	Osteoclast differentiation	17	8.63	1.38E-08
KEGG pathway	Organismal Systems	Insulin signaling pathway	17	8.63	3.70E-08
KEGG pathway	Organismal Systems	Thyroid hormone signaling pathway	16	8.12	4.49E-08
KEGG pathway	Organismal Systems	Longevity regulating pathway - multiple species	12	6.09	7.17E-08
KEGG pathway	Organismal Systems	Chemokine signaling pathway	19	9.64	1.56E-07
KEGG pathway	Organismal Systems	Growth hormone synthesis, secretion and action	15	7.61	2.50E-07

Potential mechanism of Shengxian Decoction against lung adenocarcinoma

KEGG pathway	Organismal Systems	Th17 cell differentiation	14	7.11	5.21E-07
KEGG pathway	Organismal Systems	B cell receptor signaling pathway	12	6.09	1.36E-06
KEGG pathway	Organismal Systems	Axon guidance	17	8.63	1.88E-06
KEGG pathway	Organismal Systems	Longevity regulating pathway	12	6.09	3.10E-06
KEGG pathway	Organismal Systems	GnRH signaling pathway	11	5.58	3.06E-05
KEGG pathway	Organismal Systems	PPAR signaling pathway	10	5.08	3.19E-05
KEGG pathway	Organismal Systems	IL-17 signaling pathway	11	5.58	3.36E-05
KEGG pathway	Organismal Systems	Platelet activation	12	6.09	7.43E-05
KEGG pathway	Organismal Systems	Neutrophil extracellular trap formation	14	7.11	2.39E-04
KEGG pathway	Organismal Systems	Natural killer cell mediated cytotoxicity	11	5.58	3.94E-04
KEGG pathway	Organismal Systems	Toll-like receptor signaling pathway	10	5.08	4.08E-04
KEGG pathway	Organismal Systems	GnRH secretion	8	4.06	4.41E-04
KEGG pathway	Organismal Systems	Parathyroid hormone synthesis, secretion and action	10	5.08	4.70E-04
KEGG pathway	Organismal Systems	Adipocytokine signaling pathway	8	4.06	6.99E-04
KEGG pathway	Organismal Systems	Leukocyte transendothelial migration	10	5.08	7.99E-04
KEGG pathway	Organismal Systems	Fc gamma R-mediated phagocytosis	9	4.57	1.17E-03
KEGG pathway	Organismal Systems	Th1 and Th2 cell differentiation	8	4.06	3.74E-03
KEGG pathway	Organismal Systems	Ovarian steroidogenesis	6	3.05	4.77E-03
KEGG pathway	Organismal Systems	Antigen processing and presentation	7	3.55	6.78E-03
KEGG pathway	Organismal Systems	Aldosterone-regulated sodium reabsorption	5	2.54	8.10E-03
KEGG pathway	Organismal Systems	Long-term depression	6	3.05	9.48E-03

Supplementary Table 3. Degree centrality (DC), closeness centrality (CC) and betweenness centrality (BC) values for potential targets of Shengxian Decoction (SXT) for lung adenocarcinoma

No	Target	DC	CC	BC
1	ALB	118	0.72	5615.68
2	AKT1	111	0.7	2916.85
3	EGFR	98	0.66	2002.56
4	SRC	87	0.63	1008.92
5	HSP90AA1	85	0.63	1505.92
6	CASP3	85	0.64	1347.02
7	MMP9	83	0.63	1548.34
8	HRAS	81	0.62	1041
9	ESR1	79	0.61	1281.94
10	IGF1	77	0.61	721.8
11	RHOA	68	0.58	593.45
12	MAPK1	67	0.58	817.36
13	ANXA5	61	0.58	250.16
14	PPARG	59	0.58	1161.49
15	MMP2	59	0.57	572.29
16	MAPK8	56	0.56	268.43
17	MAPK14	56	0.56	335.19
18	PIK3R1	55	0.54	207.77
19	MDM2	55	0.56	414.59
20	CDC42	52	0.54	201.01
21	KDR	51	0.54	152.06
22	CAT	50	0.55	1181.35
23	GRB2	48	0.54	128.3
24	STAT1	48	0.54	774.29
25	IGF1R	47	0.55	118.06
26	IL2	46	0.55	363.56

Potential mechanism of Shengxian Decoction against lung adenocarcinoma

27	JAK2	46	0.54	149.1
28	MAP2K1	45	0.54	140.88
29	PTPN11	44	0.53	101.52
30	KIT	44	0.54	338.16
31	AR	43	0.54	465.01
32	GSK3B	42	0.54	113.56
33	NOS3	42	0.55	197.1
34	XIAP	42	0.52	244.96
35	RAF1	41	0.53	300.17
36	PGR	41	0.54	249.64
37	PTK2	40	0.52	89.49
38	AKT2	39	0.53	210.12
39	PARP1	37	0.53	114.51
40	MET	36	0.51	58.37
41	LCK	36	0.51	40.17
42	CCL5	35	0.52	342.12
43	CDK2	35	0.53	249.63
44	ABL1	35	0.51	93.81
45	CCNA2	34	0.52	274.77
46	FGFR1	32	0.51	57.53
47	MMP3	32	0.51	107.94
48	ACE	32	0.52	187.53
49	HSPA8	32	0.52	133.69
50	CTSB	31	0.51	189.72
51	F2	30	0.51	256.39
52	RAC1	30	0.49	41.75
53	CDK6	30	0.52	96.17
54	CASP1	29	0.52	154.57
55	NR3C1	29	0.51	65.68
56	ERBB4	29	0.49	39.94
57	HSPA1A	28	0.51	38.24
58	ESR2	28	0.51	307.17
59	SELE	28	0.51	416.86
60	REN	28	0.51	94.02
61	APAF1	27	0.51	72.96
62	PIK3CG	27	0.48	19.07
63	GSTP1	27	0.52	554.7
64	MMP7	27	0.5	64.29
65	MMP1	27	0.5	41.31
66	BMP2	26	0.5	31.4
67	CTSD	26	0.5	155.13
68	RXRA	25	0.5	338.17
69	CHEK1	25	0.51	87.27
70	PLAU	25	0.5	34.41
71	NOS2	25	0.51	69.53
72	INSR	25	0.48	117.31
73	LGALS3	25	0.5	25.39
74	SYK	24	0.49	72.99
75	TYMS	24	0.49	802.53

Potential mechanism of Shengxian Decoction against lung adenocarcinoma

76	CSK	24	0.48	20.3
77	AURKA	23	0.48	166.12
78	FGFR2	22	0.47	18.35
79	TGFBR1	22	0.49	30.33
80	SOD2	22	0.5	41.08
81	EIF4E	22	0.49	54.15
82	SERPINA1	22	0.48	135.88
83	PDPK1	22	0.47	13.05
84	NQO1	22	0.51	468.95
85	RARA	22	0.48	110.47
86	PLK1	21	0.5	90.12
87	PGF	21	0.49	53.06
88	CASP7	21	0.49	31.52
89	TGFB2	21	0.48	14
90	DHFR	21	0.49	694.62
91	ELANE	20	0.48	402.72
92	VDR	20	0.49	71.8
93	SELP	20	0.49	32.28
94	EPHA2	20	0.46	9.14
95	CTNNA1	20	0.46	14.38
96	TGFBR2	19	0.49	14.84
97	TEK	19	0.48	6.93
98	BTK	18	0.45	4.43
99	JAK3	18	0.47	1.79
100	HPRT1	18	0.5	570.25
101	ARG1	18	0.49	52.42
102	DPP4	18	0.49	121.78
103	BMP7	18	0.49	198.85
104	BAG1	17	0.47	102.72
105	MMP13	17	0.48	26.47
106	CYP19A1	17	0.49	90.42
107	LCN2	17	0.48	32.24
108	CYP2C9	17	0.47	192.53
109	RHEB	16	0.46	3.65
110	SPARC	15	0.47	8.82
111	GSTM1	15	0.48	176.74
112	ADAM17	15	0.47	7.34
113	TTR	15	0.47	230.9
114	FABP4	14	0.48	88.63
115	GSTM2	14	0.48	148.08
116	MME	14	0.47	436.78
117	TK1	13	0.39	59.75
118	GC	13	0.45	44.62
119	HSPA1B	13	0.46	2.05
120	RXRB	13	0.45	53.16
121	PCK1	13	0.47	240.5
122	DUSP6	13	0.45	1.79
123	LDHB	13	0.41	133.8
124	CYP2C8	12	0.45	86.37

Potential mechanism of Shengxian Decoction against lung adenocarcinoma

125	PPIA	12	0.48	24.57
126	TGM2	12	0.48	7.42
127	NR1I2	12	0.48	66.22
128	RARB	12	0.45	97.83
129	CMA1	12	0.46	13.04
130	KIF5B	11	0.43	25.85
131	KIF11	11	0.39	20.14
132	UMPS	11	0.37	56
133	MMP12	11	0.46	12.81
134	ALDOA	11	0.46	45.81
135	SULT2A1	11	0.4	82.39
136	AKR1C3	11	0.43	56.38
137	EPHB4	11	0.44	1.89
138	CDK7	10	0.43	1.6
139	TYMP	10	0.45	147.12
140	APRT	10	0.37	70.6
141	MIF	10	0.48	76.99
142	HSD17B1	10	0.4	32.2
143	GSTA3	10	0.39	29.02
144	F7	10	0.44	11.85
145	CTSS	9	0.41	3.86
146	DAPK1	9	0.45	10.29
147	PAH	9	0.44	71.26
148	HK1	9	0.45	57.92
149	PPARD	9	0.45	39.93
150	FHIT	8	0.44	55.17
151	CTSV	8	0.43	11.95
152	DCK	8	0.36	4.23
153	FOLH1	8	0.47	82.98
154	PKLR	8	0.38	50.09
155	TNK2	8	0.45	0.77
156	STS	8	0.4	19.51
157	ADH1C	8	0.36	15.27
158	ADH1B	8	0.38	8.86
159	PAPSS1	7	0.42	12.69
160	CDA	7	0.35	17.7
161	APOA2	7	0.44	5.91
162	PLA2G2A	7	0.46	30.38
163	CES1	7	0.45	109.48
164	AKR1C2	7	0.38	46.93
165	BCHE	7	0.45	20.6
166	CRABP2	6	0.38	7.75
167	MTHFD1	6	0.35	18.92
168	BIRC7	6	0.41	0.9
169	F11	6	0.43	0.59
170	APCS	6	0.43	1.19
171	OTC	6	0.44	27.34
172	MAOB	6	0.41	31.14
173	PIM1	5	0.44	1.43

Potential mechanism of Shengxian Decoction against lung adenocarcinoma

174	NR1I3	5	0.42	8.88
175	NR1H2	5	0.39	3.24
176	AKR1C1	5	0.36	3.43
177	PLA2G10	4	0.38	2.12
178	CRYZ	4	0.38	0
179	TREM1	4	0.4	0.17
180	FABP7	4	0.39	3.01
181	CFD	4	0.43	0
182	GBA	4	0.45	20.94
183	HNF4G	3	0.34	6.55
184	BHMT	3	0.35	0
185	B3GAT1	3	0.38	0.8
186	MTAP	3	0.35	5.05
187	FAP	2	0.37	0
188	ISG20	2	0.37	0
189	CLEC4M	2	0.44	0
190	TAP1	1	0.35	0
191	QPCT	1	0.32	0
192	LGALS7B	1	0.34	0
193	PADI4	1	0.32	0

Supplementary Table 4. Binding energies of the seven active components of Shengxian Decoction to the 13 key targets.

No	Target	Calycosin 7-O-glucosid binding energy (kJ·mol ⁻¹)	Formonone- tin binding energy (kJ·mol ⁻¹)	Neomangif- erin bind- ing energy (kJ·mol ⁻¹)	Mangifer- in binding energy (kJ·mol ⁻¹)	Saikosapo- nin A bind- ing energy (kJ·mol ⁻¹)	Luteolin binding energy (kJ·mol ⁻¹)	Isoferulic acid bind- ing energy (kJ·mol ⁻¹)
1	ALB	-10.1	-9.5	-8.5	-9.7	-7.8	-9.7	-7.3
2	AKT1	-10.7	-9.7	-10.7	-9.5	-8.7	-9.3	-6.8
3	EGFR	-8.4	-7.8	-9.1	-8.5	-8.5	-8.7	-6.2
4	SRC	-9.5	-8.7	-8.5	-8.4	-7.6	-6.3	-6.4
5	HSP90AA1	-7.6	-7	-7.5	-7	-7.4	-6.2	-6.2
6	CASP3	-7.5	-7	-8.1	-7.1	-8.5	-7.3	-5.6
7	MMP9	-9.6	-10.5	-7.9	-10.4	-8.5	-10.1	-8.2
8	HRAS	-9.5	-8	-8.3	-8.8	-6.8	-9	-6.7
9	ESR1	-7.9	-6.4	-8.4	-6.5	-7.4	-7.5	-6.1
10	IGF1	-8.7	-7.6	-9	-8.3	-8.3	-6.6	-5.9
11	RHOA	-8.6	-6.9	-7.8	-7.9	-7.6	-7.8	-6.7
12	MAPK1	-9.3	-7.7	-10.2	-8.3	-9.3	-7.9	-6
13	ANXA5	-8.6	-7.6	-8.6	-8	-7.9	-7.1	-6.2

ALB, albumin; AKT1, serine/threonine protein kinase 1; EGFR, epidermal growth factor receptor; SRC, steroid receptor coactivator; HSP90AA1, heat shock protein 90 alpha family class A member 1; CASP3, caspase-3; MMP9, matrix metalloproteinase-9; HRAS, harvey rat sarcoma viral oncogene homolog; ESR1, estrogen receptor 1; IGF1, insulin like growth factor 1; RHOA, ras homolog gene family member A; MAPK1, mitogen-activated protein kinase 1; ANXA5, annexin A5.